



A two-phase and long-lasting multi-antibacterial coating enables titanium biomaterials to prevent implants-related infections



Ruitian Lin^{a,b}, Zhuoran Wang^{a,b}, Zihan Li^{a,b}, Lisha Gu^{a,b,*}

^a Hospital of Stomatology, Guanghua School of Stomatology, Sun Yat-sen University, China

^b Guangdong Provincial Key Laboratory of Stomatology, China

ARTICLE INFO

Keywords:

Implant coating
Multi-antibacterial property
Osteogenicity
Modified layer-by-layer self-assembly
Dopamine polymerization

ABSTRACT

In clinical work, the main challenges for titanium (Ti) implantation are bacterial infection and aseptic loosening, which severely affect the survival rate of implants. The first 4 weeks post-operation is the infection peak phase of implants. Inhibiting implant infection caused by bacteria adhesion and proliferation during the early phase as well as promoting subsequent osteointegration is essential for implant success. Herein, we constructed a quaternary ammonium carboxymethyl chitosan (QCMC), collagen (COL I) and hydroxyapatite (HAP) multilayers coating on Ti substrates via a modified layer-by-layer (LBL) technique and polymerization of dopamine. The QCMC/COL/HAP coating exhibited a multi-antibacterial property with a two-phase function: (1) At the first 4 weeks post-operation, the covalently bonded QCMC could be slowly degraded and demonstrated both contact-killing and release-killing properties during the infection peak phase; (2) At the second phase, osteogenesis and osseointegration-promotion capabilities were enhanced by HAP under the effective control of infection. The multilayer coating was degraded for more than 45 days under the action of collagenase I, and displayed good biocompatibility *in vivo* and *in vitro*. Most importantly, the coating exhibited a long-lasting antibacterial activity for more than 3 months, against the main pathogenic bacteria of peri-implant infections. Both *in vitro* studies and *in vivo* animal models revealed a desirable osteogenic differentiation capacity of Ti-CCH. Therefore, our study reports a two-phase, long-lasting multi-antibacterial coating on Ti-CCH and indicates potential applications of the modified LBL strategy in orthopaedic fields, which is enlightening for developing practical implant and scaffold materials.

1. Introduction

Titanium (Ti) and its alloy have been extensively used as orthopaedic implants for their excellent mechanical properties, good biocompatibility and superior erosion resistance. During tooth implant surgery, a thoroughly sterile environment is difficult to obtain since over 600 bacterial species harvest in oral cavity [1]. Planktonic bacteria may adhere to the Ti surface during the screwing process or enter the tissue wound after operation. Once a structured biofilm has formed on the implant surface, it protects adherent bacteria from the host defence system and external therapeutic agents via several mechanisms, which eventually leads to implant failure [2–4]. Although structural modifications such as sand-blasting and acid etching have been widely used clinically to improve the bioactivity of pure Ti, it is limited to endow the implant with desirable antibacterial functions [5]. Moreover, it was reported that the incidence of infection for Ti implants was about 10%, and nearly two-thirds of

infected implants failed before functional loading [6]. Therefore, the shortcomings of structural modifications are driving the development of biological coatings on Ti. Recently, progress has been made to reduce bacterial adhesion and biofilm formation through various bioactive coatings in order to prevent implant infection and failure [7–9]. Nevertheless, Ti coatings utilizing un-covalent bonding such as electrostatic interaction and hydrogen bond, were not stable and were quickly degraded during the early phase after implantation [10,11]. On the other hand, Ti coatings using traditional covalent bonding might undergo a burst release of antibacterial agents, and only maintain a deficient concentration for killing bacteria in a later phase [12]. The infection peak phase of the implant remains for 4 weeks post-operation, while the total stability of implants reaches to a steady state at the eighth week after implantation and becomes completely stable until 3 months [13,14]. As a consequence, all of the above methods could not promise the implant surface with stable and effective antibacterial properties over time.

* Corresponding author. Hospital of Stomatology, Guanghua school of Stomatology, Sun Yat-sen University, No. 56, Lingyuan West Road, Guangzhou, China.
E-mail address: gulisha@mail.sysu.edu.cn (L. Gu).

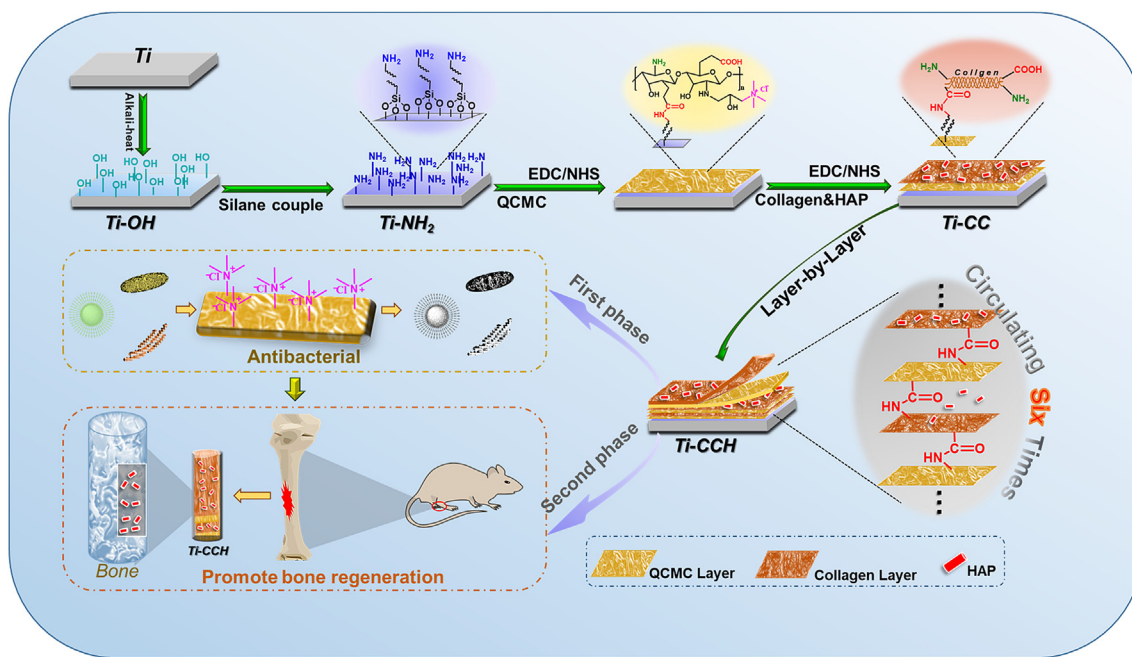


Fig. 1. Schematic illustration of construction of the QCMC/COL I/HAP coating on Ti-CCH and its two-phase effects.

To confer the implant with desirable properties, different methods such as plasma spraying, anodization and layer-by-layer (LBL) technique have been deeply investigated to fabricate bioactive coatings [4,15,16]. Among them, LBL has been proved to be a highly effective method to immobilize multi-components of the extracellular matrix (ECM) on biomaterials since reported by Decher et al. [17]. Nevertheless, the interactions responsible for the LBL multifilm were largely electrostatic, which was unstable under physiological condition [18]. Recently, Ao et al. [19,20] proposed a modified LBL technique to develop multifilm structure with amido bond crosslinking. The reaction between carboxyl and amino groups was catalyzed by EDC/sulfo-NHS crosslinker to form the LBL multifilm structure. Compared to the conventional LBL technique which utilized electrostatic interaction and physical crosslinking, the modified LBL multifilm was stable in tris-buffer and degraded slowly under the action of collagenase solution. This indicated that the modified LBL technique could be applied in developing antibacterial coatings to obtain long-lasting, release-killing and contact-killing properties. To endow implants with effective antibacterial activity, a large number of antibacterial agents have been utilized such as antibiotic, graphene oxide, nano-silver, chitosan, etc. [7,9,21]. Chitosan is a natural polymer widely used in tissue engineering and drug delivery system due to its biocompatibility, biodegradability, bioadhesivity as well as bioactivity [12]. As a chitosan derivative, quaternary ammonium carboxymethyl chitosan (QCMC) is an ideal water-soluble antibacterial agent, in which a large number of carboxyl and amino groups has been considered beneficial for the construction of covalently bonded multifilms [11,22].

Implant-related infection often occurs in the first 4 weeks post-operation [13]. In this phase, desirable antibacterial materials are needed for the prevention and control of infection. Moreover, osseointegration and the second stability of implants starts building during the end of this phase, which is essential for the improvement of total stability of implant and the final implant success. Thus, after the first 4 weeks of implantation, good osseointegration-promotion capability as well as acceptable antibacterial activity is required. Immobilizing enzymes, cytokines or main components of ECM on biomaterial surfaces have shown considerable role in inducing particular cell responses and strengthening the tissue-implant interface [20]. In this study, collagen (COL) and hydroxyapatite (HAP) were utilized to mimic the ECM of natural bone and induce osseointegration [23–25]. Both QCMC and COL were chemically

crosslinked, and HAP was bonded using poly dopamine as binding agents [26,27]. The QCMC/COL/HAP multilayer coating might endow the implant with a long-lasting, multi-antibacterial property and a two-phase function. At the first 4 weeks post-operation, the covalently bonded QCMC could be slowly degraded. The degraded QCMC exhibited release-killing effect and the remaining QCMC in coatings could achieve contact-killing property during the infection peak phase; then during the second phase, osteogenesis and osseointegration might be promoted due to the osteoinductivity of HAP. The null hypotheses tested were: 1) The QCMC/COL/HAP multilayer structure can not be constructed via modified LBL technique and poly dopamine binding methods. 2) QCMC can not be slowly degraded from the multilayer structure for a long period of time. 3) The QCMC/COL/HAP multilayer structure has no long-lasting, multi-antibacterial effects and a two-phase function.

2. Experimental section

2.1. Materials

Ti disc (10 mm*10 mm*0.5 mm) and rod (10 mm*Φ1mm) were obtained from Sante Material (Taizhou, China). Carboxymethyl chitosan (CMC), 2-Morpholinoethanesulphonic acid (MES) buffer, dopamine hydrochloride and cetylpyridinium chloride were purchased from Solarbio (Beijing, China). EDC (1-ethyl-3-(3-dimethylaminopropyl) carbodiimide hydrochloride), sulfo-NHS (N-hydroxysulfosuccinimide) and type-I collagenase were obtained from Sigma-Aldrich (St. Louis, MO, USA). Rat tails were provided by the Experimental Animal Center. Cell Counting Kit-8 (CCK-8) was purchased from Dojindo (Shanghai, China). DAPI dye solution was purchased from Beyotime (Shanghai, China). Minimum Essential Medium alpha basic (α -MEM), Fetal Bovine Serum (FBS) and phosphate balanced solution (PBS) were provided by GIBCO (Grand Island, USA). Bicinchoninic acid (BCA) protein assay kit was obtained from Comwin (Beijing, China). Alkaline phosphatase (ALP) assay kit was purchased from Jianchen (Nanjing, China). Brain heart infusion broth (BHI) was purchased from HuanKai Microbial (Guangdong, China). Osteogenic differentiation medium was purchased from Cyagen (Suzhou, China). Hematoxylin-eosin staining kit was purchased from Biosharp (Beijing, China). Other chemical reagents were obtained from Macklin (Shanghai, China). *Staphylococcus aureus* (ATCC 25923), *Staphylococcus*

Table 1

The grouping details in each experimental section.

| Experimental section | Groups | Numbers of rats | Micro-CT analysis and Bone histopathology | Microbiological evaluation | Weight and blood detection | Time for sacrifice |
|----------------------|------------------|-----------------|---|--|----------------------------|--------------------|
| Biocompatibility | Ti-OH | 5 | 5 femurs with implants | – | All of rats | 6 weeks |
| | Ti-CCH | 5 | | | | |
| Anti-infection | Ti-OH+PBS | 10 | 5 femurs with implants | 5 implant rods and 5 weighed femurs for quantitation | – | 4 weeks |
| | Ti-OH+S. aureus | 10 | | | | |
| | Ti-CCH+S. aureus | 10 | | | | |
| Pro-osteogenesis | Ti-OH+PBS | 5 | 5 femurs with implants | – | – | 8 weeks |
| | Ti-OH+S. aureus | 5 | | | | |
| | Ti-CCH | 5 | | | | |
| | Ti-CCH+S. aureus | 5 | | | | |

– represent no treatment.

epidermidis (ATCC 12228) and *Enterococcus faecalis* (ATCC 29212) were obtained from Microbial Culture Collection Center.

2.2. Methods

2.2.1. Synthesis and characterization of QCMC and COL I

The synthesis of QCMC was described in the literature [28]. Briefly, 5 g CMC was completely dissolved in double-distilled water (ddH₂O) and (3-Chloro-2-hydroxypropyl) trimethylammonium chloride (CTA) were slowly dropped into CMC solution. The mixture solution was stirred at 80 °C for 8 h, followed by dialysis against pure water for 5 days and lyophilization. In this study, CMC was a long-chain polymer with repeating units and functioned as a reactant to synthesize QCMC. The repeating unit in CMC was called as “chitosan oligosaccharide unit”. In order to explore the optimal reactant proportion of CTA and CMC, different molar ratios of CTA to chitosan oligosaccharide units from 3:1 to 6:1 were employed. COL I was extracted from rat-tail tendons and dissolved in 0.2% acetic acid, followed by dialysis against dipotassium hydrogen phosphate solution and lyophilization [29]. Fourier transform infrared (FTIR; Nicolet 6700, Thermo Scientific, USA) spectroscopy was used to characterize the synthetic QCMC and COL I. Elemental analysis (Vario EL cube, Elementar, Germany) was used to evaluate the content of nitrogen (N) and carbon (C) elements in QCMC synthesized using a series proportion of CTA. The substitution degree of quaternary ammonium groups was calculated as described in Supplementary information.

2.2.2. Construction of Ti-CCH coating

The modified multilayer structures were constructed by the LBL technique as described in the literature (Fig. 1) [20]. Firstly, Ti substrates were immersed in 5 M NaOH solution at 80 °C for 12 h, ultrasonically cleaned and dipped in deionized water at 60 °C for 7 days with the water changed daily, then the Ti was named Ti-OH. A 95% ethanol solution was prepared and the pH was adjusted in a range from 4.5 to 5.5 using acetic acid. Five volume percent of silane coupling agent KH550 was hydrolyzed in the pH-adjusted ethanol solution and the mixture was placed for 5 min at room temperature. Then Ti-OH substrates were immersed into the aforementioned solution with continuously magnetic stirring for 2 h, followed by ethanol washing and vacuum drying at 110 °C for 30 min. After silane coupling treatment, the Ti-OH was named Ti-NH₂.

Afterward, the modified LBL self-assembly coating was constructed by EDC/sulfo-NHS crosslinkers [19]. Firstly, 5 mg/mL QCMC and 1 mg/mL COL solutions were prepared respectively, and the pH was adjusted to 5.0 by using MES buffer. Then 2.5 mg/mL EDC was added into QCMC solution and stirred for 10 min to activate carboxyl groups. In order to stabilize carboxyl groups, 0.63 mg/mL sulfo-NHS was added and the pH was adjusted to 7.2–7.5 with PBS immediately. Thereafter, Ti-NH₂ samples were immersed into above QCMC solution and stirred for 15 min. The methods for grafting COL were the same as that of QCMC. After crosslinked with QCMC and COL, the Ti-NH₂ was named Ti-CC. Then HAP was added using self-polymerization method as described in

the literature [13]. Briefly, Ti-CC substrates were immersed into 50 mM tris-buffer (pH = 8.5). Then 5 mg/mL HAP and dopamine hydrochloride were added separately, vibrating for 24 h. The above steps of coating QCMC, COL and HAP were treated as one cycle, and a total of six cycles were performed. After the coating completed, Ti-CC were named Ti-CCH.

2.2.3. Characterization of Ti-CCH coating

The characterizations of the samples were performed at different steps of fabricating the coating. Scanning electron microscopy (SEM; Merlin, Zeiss, Germany) was employed to observe the surface morphology of Ti coating in each step of construction and the thickness of the final coating. X-ray photoelectron spectroscopy (XPS; Escalab 250, Thermo-VG Scientific, USA) was then performed to analyze the elemental components and valence states on the Ti surface. Water contact angle measurement (OCA40 Micro, Dataphysics, Germany) and confocal laser scanning microscope (CLSM; LSM700, Zeiss, Germany) were employed to evaluate the hydrophilicity and surface roundness of different Ti substrates. Young's modulus of Ti-CCH was measured by atomic force microscopy (Dimension fastscan bio, Bruker, Germany) in the peak force quantitative nanomechanics mode and was analyzed by the Derjaguin–Muller–Toporov model. To further evaluate the mechanical stability of QCMC/COL/HAP coating, Scratch test and SEM were employed to evaluate the mechanical stability of QCMC/COL/HAP coating on Ti-CCH.

2.2.4. Biocompatibility and biodegradability of Ti-CCH coating

The proliferation rate of MC3T3 E1 osteoblastic cells after co-cultured with Ti-OH and Ti-CCH samples for 1, 3 and 7 days was measured using CCK-8 assay. Fluorescent actin staining assay was conducted to evaluate the cell adhesion to Ti-OH and Ti-CCH surface. The release of QCMC was detected by anthrone–sulfuric acid reaction, using glucose as a standard. Briefly, Ti-CCH substrates were immersed into 2 mL collagenase solution (1 mg/mL collagenase I and 50 mmol/L tris-HCL) and 50 mmol/L tris-HCL separately and incubated in 37 °C for 45 days. The solutions were collected and renewed every 2 days, following the anthrone-sulfuric acid detection [19].

Twenty-week-old Sprague Dawley (SD) rats were employed to build femur implant models for evaluating the biocompatibility of Ti-CCH. Ten SD rats were randomly divided into two groups. The grouping details of each experimental section can be seen in Table 1. Ti-OH and Ti-CCH rods (n = 5) were implanted into the left femurs of the rats as described in previous studies [30,31]. Briefly, the rats were anesthetized, the distal femur and intercondylar fossa were then exposed. Dental drill was used to make a 1-mm-diameter, 10-mm-depth hole through the intercondylar fossa, then a rod with or without infection was placed into the hole. The incision was sutured in layers. The body weight of rats per group was measured weekly, and venous blood samples were collected 3 and 6 weeks after surgery, neutrophil (NE) and hemoglobin (HGB) of the blood samples were measured. After implantation for 6 weeks, rats were sacrificed by cervical vertebrae. Femurs were removed and immersion-fixed in 4% paraformaldehyde in PBS upon collection and

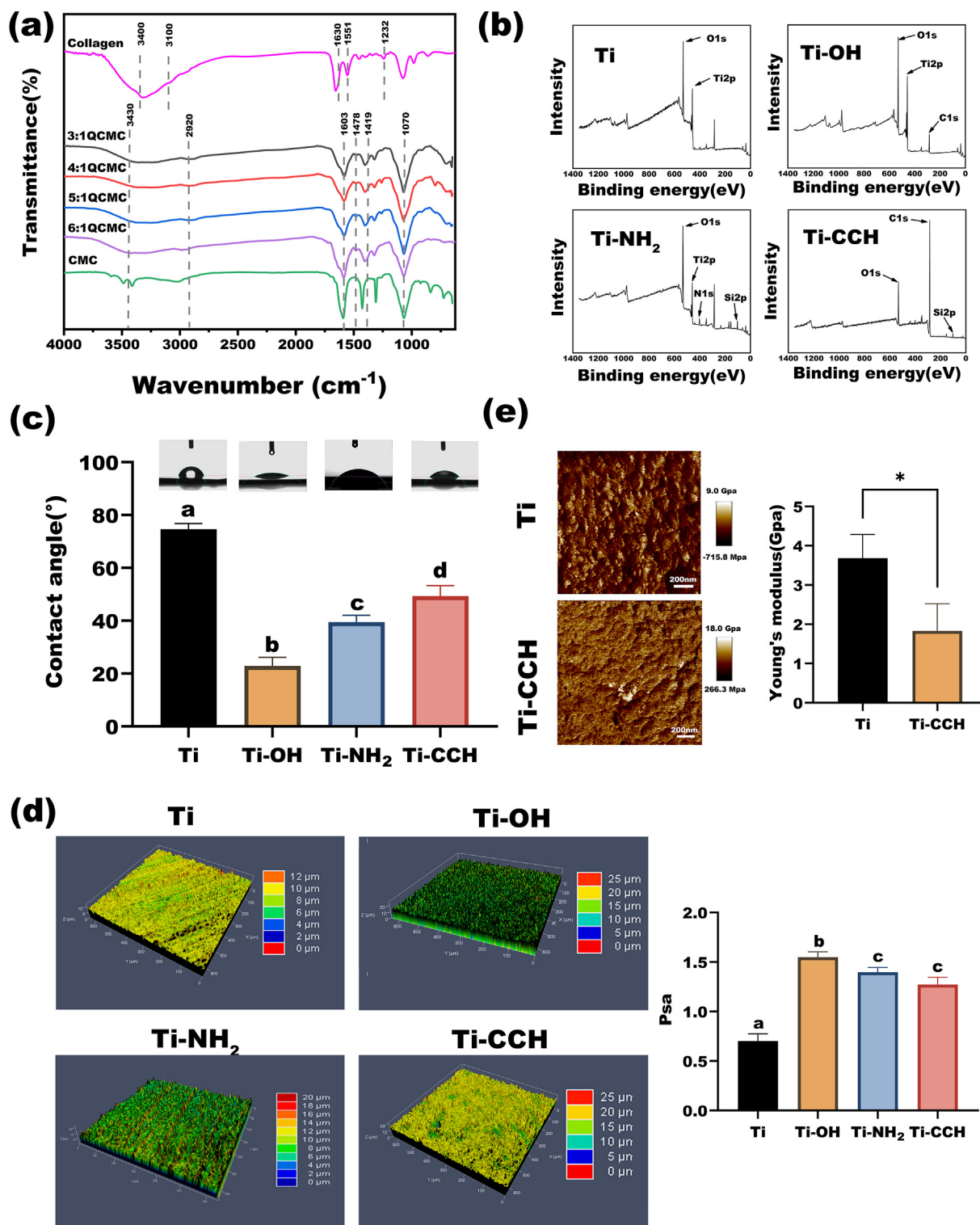


Fig. 2. Characterization of the synthetic QCMCs, COL I and QCMC/COL I/HAP multifilm coating on the titanium surface. (a) FTIR spectra of the synthetic QCMCs and COL I. (b) XPS spectra of Ti, Ti-OH, Ti-NH₂ and Ti-CCH. (c) Water contact angle of Ti, Ti-OH, Ti-NH₂ and Ti-CCH (n = 3). (d) CSLM images of the surface roughness of Ti, Ti-OH, Ti-NH₂ and Ti-CCH (n = 3). (e) Young's modulus mapping via AFM of Ti and Ti-CCH. Different lowercase superscript letters indicate significant differences (n = 3). *P < 0.05.

then transferred into 75% ethanol after 24 h. The femurs samples were scanned and bone morphometry was analyzed using a Micro-CT scanner (Inveon PET/CT, Siemens, Germany). After Micro-CT scanning, the femurs were decalcified in 0.5 mol/L EDTA solution for 3 weeks. The implants in femurs were removed and underwent paraffin embedding, section, followed by hematoxylin and eosin (HE) staining.

2.2.5. Long-lasting and multi-antibacterial activity assessments

ATCC 25923, ATCC 29212 and ATCC 12228 were employed to study the antibacterial properties of Ti-CCH. The concentration of bacteria was adjusted to 10⁶ CFU/mL and the contact and release-antibacterial activity was evaluated by spread plate method [32]. It was known that the contact ability of bacteria was relatively influenced by the surface

properties of biomaterials. Since the surface of Ti-OH was similar to Ti-CCH's, we used Ti-CCH and Ti-OH as experimental and control groups separately to evaluate the contact-antibacterial activity of Ti-CCH. The contact ability of bacteria on titanium substrate was studied so that there was no control check group in this section. Briefly, Ti-CCH and Ti-OH substrates were cocultured with 2 mL each bacteria suspension at 37 °C for 12 and 24 h, followed by ultrasonically washing with 3 mL PBS. Then the bacteria suspensions were serially diluted 100-fold, plated onto BHI plate and incubated for 24 h. To investigate the release-antibacterial activity, BHI, Ti-OH+BHI+type I collagenase, Ti-CCH+BHI+type I collagenase were separately co-cultured at 37 °C for 24 h and the solutions were filter sterilized. Ten microliter of 10^6 CFU/mL of three bacteria suspensions were added into 1 mL of above solutions, incubated at 37 °C with shaking at 150 rpm for 24 h and evaluated by spread plate method. The inhibition effect of Ti-CCH on biofilm formation was further assessed by SEM. Live/dead staining was conducted to further study the antibacterial activity of Ti-CCH. The evaluation of long-lasting antibacterial activity of Ti-CCH was conducted with spread plate method as described in the previous study, in which *S. aureus* was utilized as representative [33]. Briefly, Ti-OH and Ti-CCH substrates were stored at sterile PBS for 0, 3, 6, 9 and 12 weeks separately. The samples were transferred to 24-wells-plate at each designated time and co-cultured with 2 mL of 10^6 CFU/mL *S. aureus* suspensions at 37 °C for 24 h, followed by ultrasonically washing with 3 mL PBS. Then the bacteria solutions were serially diluted 100-fold, plated onto BHI plate and incubated for 24 h.

2.2.6. Anti-infection evaluation of Ti-CCH

The femur implant infection model was constructed as described in previous study [13]. Briefly, Ti-OH and Ti-CCH rods were immersed into PBS or 10^6 CFU/mL of *S. aureus* suspension for 10 min. Then Ti-OH and Ti-CCH rods were implanted into the left femurs of rats as mentioned before. The grouping details are shown in Table 1. After implantation for 4 weeks, rats were sacrificed by cervical vertebrae. The implants of 15 rats were removed in a bacteria-free environment and ultrasonically cleaned in PBS for 5 min, followed by gradient diluted for bacterial colony counting. After implants removal, the femurs were weighed, frozen in liquid nitrogen and were grounded into powder. The powder was ultrasonically cleaned in PBS for 5 min, followed by gradient diluted for bacterial colony counting. Quantitation of bacteria in bone tissues was calculated by CFU/g. In addition, Femurs of the other 15 rats were removed and immersion-fixed in 4% paraformaldehyde in PBS upon collection and then transferred into 75% ethanol after 24 h. The femurs samples were scanned, and bone morphometry was analyzed using a Micro-CT scanner. Then femurs were decalcified in 0.5 mol/L EDTA solution for 3 weeks. The implants in femurs were removed and underwent paraffin embedding, section, followed by hematoxylin and eosin (HE) staining.

2.2.7. Assessment of osteogenesis abilities

MC3T3 E1 osteoblastic cells were employed to evaluate the osteogenesis property of Ti-CCH by using ALP activity detection and Alizarin red staining. Briefly, MC3T3 E1 cells were adjusted to a density of 5×10^4 /mL, and were cocultured with Ti-OH and Ti-CCH respectively for 7 and 14 days with osteogenic induction. The ALP activity and total protein concentration in the cell lysates were measured by using a microplate reader at a wavelength of 562 nm. Mineralized nodules were visualized by Alizarin red staining after coculturing for 28 days with osteogenic induction. Ten percent of cetylpyridinium chloride was added to dissolve the stain for the quantitative assay.

The femur implant infection model was constructed as mentioned above. After implantation for 8 weeks, rats were sacrificed by cervical vertebrae. Femurs of 15 rats were removed and immersion-fixed in 4% paraformaldehyde in PBS for 24 h upon collection, followed by 75% ethanol. The femurs samples were scanned, and bone morphometry was analyzed by using a Micro-CT scanner. Then femurs were decalcified in

Table 2

Elemental analysis and grafting ratio of quaternary ammonium groups in QCMCs.

| CTA:Glucose unit | Element content (%) | | C/N ratio | Grafting ratio (%) |
|------------------|---------------------|------|-----------|--------------------|
| | C | N | | |
| 3:1 | 38.14 | 5.61 | 6.80 | 87.5 |
| 4:1 | 38.81 | 5.76 | 6.74 | 94.54 |
| 5:1 | 37.88 | 5.60 | 6.76 | 92.14 |
| 6:1 | 36.96 | 5.46 | 6.77 | 90.96 |
| CMC | 30.38 | 3.68 | 8.25 | – |

CTA: (3-Chloro-2-hydroxypropyl) trimethylammonium chloride; CMC: carboxymethyl chitosan; N: nitrogen; C: carbon; – represents no data.

0.5 mol/L EDTA solution for 3 weeks. The implants in femurs were removed and underwent paraffin embedding, section, followed by hematoxylin and eosin (HE) staining.

2.3. Statistical analysis

Data were expressed as the mean \pm standard deviation. Statistical analysis was evaluated by SPSS 20.0 (IBM Corp., Chicago, USA) with Student's *t*-test and one-way analysis of variance (ANOVA) followed by Bonferroni multiple comparisons for data with homogeneity of variance, and Wilcoxon's nonparametric test for data with heterogeneity of variance. $P < 0.05$ was considered statistically significant.

3. Results and discussion

3.1. Synthesis and characterization of QCMC and COL I

As a novel promising chitosan derivative, QCMC was given considerable attentions and confirmed to be a functional polymer, which contained a great number of bioactive groups [22]. To synthesize QCMC, carboxymethyl and quaternary ammonium groups were grafted to chitosan to enhance its water solubility and antibacterial property. It is known that the ECM of natural bone consists of abundant COL I, which provides the structural scaffold and forms the organic matrix [23]. In order to mimic the natural bone micro-environment and endow the implant with promising antibacterial property, QCMC and COL I were synthesized for constructing implant coating according to previous studies [28]. The FT-IR spectra of COL I and QCMC are presented in Fig. 2a. The main absorption bands of CMC were 3430 cm^{-1} (O–H stretch), 2920 cm^{-1} (C–H stretch) and 1070 cm^{-1} (C–O stretch), while 1603 cm^{-1} and 1419 cm^{-1} were assigned to the asymmetric and symmetric stretching vibrations of –COOH groups, respectively. Compared to CMC, a new absorption peak at 1478 cm^{-1} emerged in the absorption bands of QCMC, indicating that quaternary ammonium group was successfully grafted to CMC [22,34]. Furthermore, QCMC had been characterized by NMR in our previous study, which proved the grafting of quaternary ammonium group [35]. The three main bands of the synthetic COL I were 1630 cm^{-1} , 1551 cm^{-1} , and 1232 cm^{-1} , related to amide I, II, and III, respectively. The peaks found in the region between 3100 cm^{-1} and 3400 cm^{-1} occurred due to the O–H and N–H stretching of amide A, indicating that COL I was successfully synthesized. In order to obtain QCMC with the maximum grafting yield, a series of experiments utilizing different reactant ratios were conducted. The graft ratios of quaternary ammonium group were calculated according to the content of C and N elements in different QCMCs. The results of elemental analysis showed that the grafting ratio of quaternary ammonium group was at its highest, reaching 94.5% when the molar ratio of CTA/chitosan oligosaccharide unit was 4:1 (Table 2). Therefore, QCMC with the highest grafting ratio has been used for the following study to obtain a higher antibacterial activity of coating.

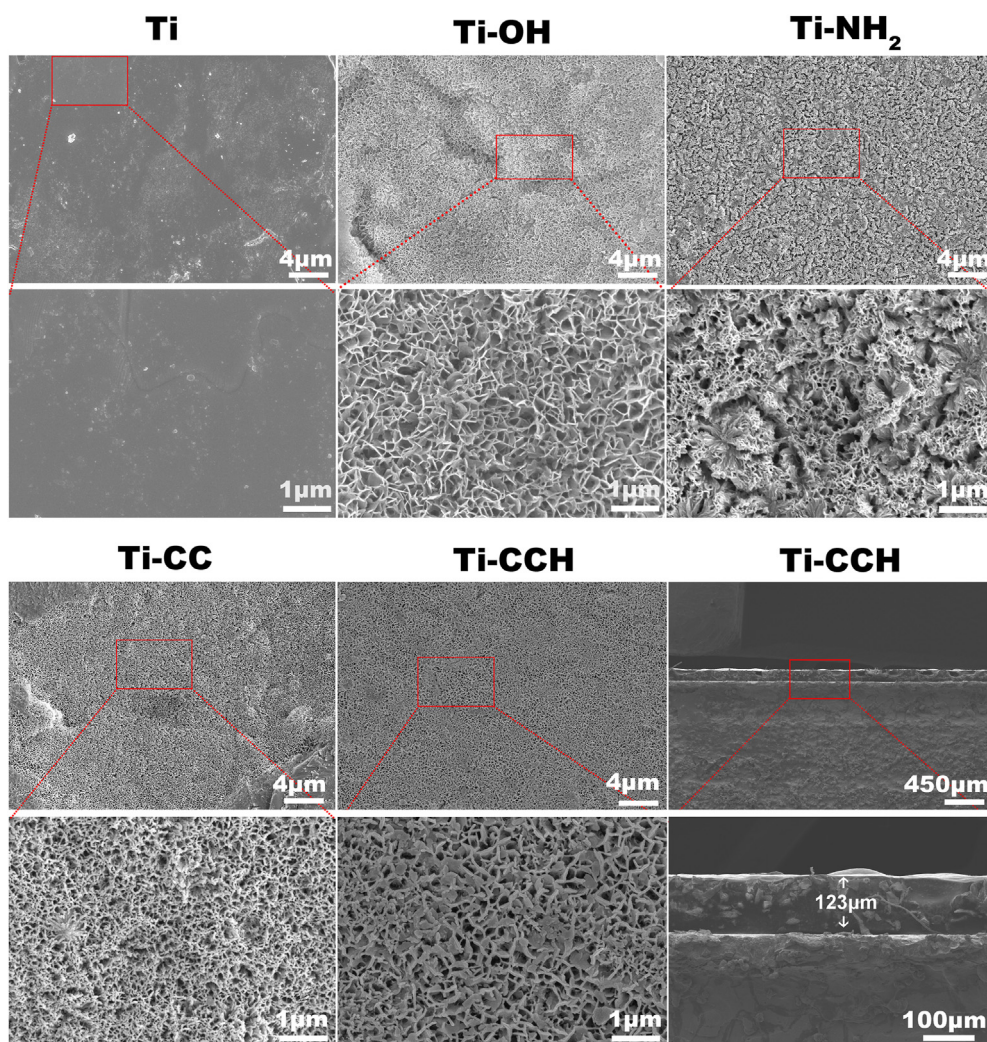


Fig. 3. SEM images showing the surface morphology of Ti, Ti-OH, Ti-NH₂, Ti-CC, Ti-CCH and the thickness of the multifilm coating on Ti-CCH.

3.2. Fabrication and characterization of Ti-CCH

The modified LBL technique and polymerization of dopamine were proved to be highly effective methods for immobilizing macromolecular on biomaterials [13,36]. In the present study, QCMC, COL I and HAP were grafted into the multifilm structure. It was known that pure Ti was an inert metal without sufficient bioactive [37]. Therefore, essential pre-treatments such as alkali-heat treatment and silane coupling were conducted in order to form stable bonds among QCMC, COL I and Ti surface. After alkali-heat treatment, XPS revealed that the O1s signal of Ti-OH increased significantly, with a binding energy over 531 eV, which belonged to hydroxyl groups (Fig. 2b). The considerable amount of polar grafted hydroxyl groups could react with water and form hydrogen bonds [38]. Accordingly, the surface of Ti-OH was the most hydrophilic with a contact angle around 23° (Fig. 2c). After silane coupling, the hydroxyl groups could react with the coupling agent and eventually form amide groups on the Ti surface, which was proved by the typical N1s peak with binding energy among 399–400 eV in XPS. Moreover, compared to the smooth surface of Ti, Ti-OH showed a palisade structure with increased surface roundness (Psa value = 1.548) after alkali-heat treatment. Then a disordered 200–400 nm wide nano-grid structure on Ti-NH₂ was observed with a slightly decreased surface roundness (Psa value = 1.397) after silane coupling (Figs. 2d and 3). The bioactivity of Ti surface was improved so that QCMC could react with amino groups on Ti-NH₂ surface, catalyzed by EDC/NHS crosslinkers. It was worth noting

that Ti-CCH still maintained the nano-grid structure with a thicker pore wall and smaller pore size around 50–200 nm after macromolecules covering, with a thickness of 123 μm (Fig. 3). The nano-grid structure generated a great special surface area, providing additional conjugation sites for biomolecules as well as cells, which have been reported to be beneficial for the adhesion and proliferation of osteoblast [39,40]. Moreover, HAP with a diameter around 200 nm was deposited in the pore and uniformly distributed among the substrate surface of Ti-CCH, which could mimic the natural bone micro-environment and induce adhesion and proliferation of osteoblasts [23]. However, characteristic peak of calcium and phosphorus element of HAP was not observed in XPS. As an energy spectrometry technique, XPS was used to determine the composition, chemical formula and electronic states of elements contained in materials with high sensitivity. Nevertheless, the detection is limited to 1–10 nm below the surface of materials and the detection region was elliptic with a long axis of 400 μm, which was randomly selected. In the LBL multifilm, HAP particles were crosslinked in the nano-grid structure, and dopamine could self-aggregate and adhere on the titanium surface while grafting HAP. Therefore, calcium and phosphorus elements in HAP might be covered by other macromolecules and could not be detected effectively using XPS. Since part of hydroxyl groups were covered by biomolecules, the hydrophilicity of Ti-CCH decreased with an increase of contact angle to 50°, though which was still lower than that of Ti (contact angle around 75°, Fig. 2c). A hydrophilic surface is beneficial for cells adhesion and decreasing bacteria attachment, which

Table 3
Element contents on different Ti substrates evaluated by XPS.

| | Element content (%) | | | | |
|--------------------|---------------------|------|-------|------|-------|
| | C | N | O | Si | Ti |
| Ti | 35.32 | 3.07 | 39.43 | 2.2 | 16.54 |
| Ti-OH | 26.49 | 0.96 | 49.07 | 1.23 | 18.23 |
| Ti-NH ₂ | 37.87 | 4.04 | 38.12 | 8.38 | 7.1 |
| Ti-CCH | 78.78 | 2.16 | 13.53 | 3.35 | 0 |

C: carbon; N: nitrogen; O: oxygen; Si: silicon; Ti: titanium.

are crucial for tissue healing and implant integration [41]. It was reported that a contact angle between 35° and 80° has been considered beneficial for bone regeneration, with 55° reported as the optimum for cell adhesion and proliferation [42]. Therefore, Ti-CCH showed a desirable surface property for attracting cells adhesion and proliferation.

Young's modulus test of Ti-CCH was conducted to evaluate the biomechanical compatibility of coatings [43]. As shown in Fig. 2e, the Young's modulus of Ti was around 3.7 Gpa, which subsequently decreased to around 1.8 Gpa after QCMC/COL/HAP coating constructing. It has been reported that the Young's modulus of periodontal ligaments of natural tooth is around 68.9 Mpa [44]. This result indicated that the Young's modulus of the coating on Ti-CCH was closer but still much higher than periodontal ligament compared to Ti. Therefore, the biomechanical compatibility of Ti-CCH still needs to be improved. Further studies should concentrate on the influence factors of the Young's modulus, including the number of multilayer layers, the concentration of

reactants and reaction time, to optimize the biomechanical compatibility of Ti-CCH. Apart from the visualized evidence from SEM, the surface elements and their valence states evaluated by XPS also confirmed the successful construction of QCMC/COL/HAP multilayer coating (Table 3 and Fig. S1). After crosslinking, Ti-CCH showed an obvious C1s peak at around 288 eV, representing the grafting of carboxyl groups. The disappearance of Ti2p peak and weakening of Si2p peak indicated the decreasing of the content of Ti and Si elements on Ti-CCH surface, which was a result of LBL films covering. Moreover, the carbon (C) content increased from 26.49% to 78.78% and Ti content decreased from 18.23% to 0% during the coating process. The content of silane (Si) increased and was at its highest, reaching 8.38% after silane coupling, followed by a decrease to 3.35% when covering QCMC, COL and HAP. The above results revealed that multilayer structures were successfully constructed. However, due to the aforementioned deficiency of XPS technique, the grafting degree of QCMC on Ti-CCH could not be calculated. The amount of QCMC on Ti-CCH was further evaluated in the degradation experiment.

When the Ti-CCH implants are implanted into the body, the surrounding bone tissue will generate mechanical friction on the surface of the implanted material. Therefore, we conducted the scratch test to evaluate the mechanical stability of QCMC/COL/HAP coating. In the scratch test, parameters such as probing depth (Pd), scratching time, force of friction (Ft) and acoustical emission (AE) were continuously recorded with the increasing of scratch length. These parameters would undergo an abrupt change when the coating was broken. Therefore, the binding force of coating could be evaluated and Fig. 4a shows the change

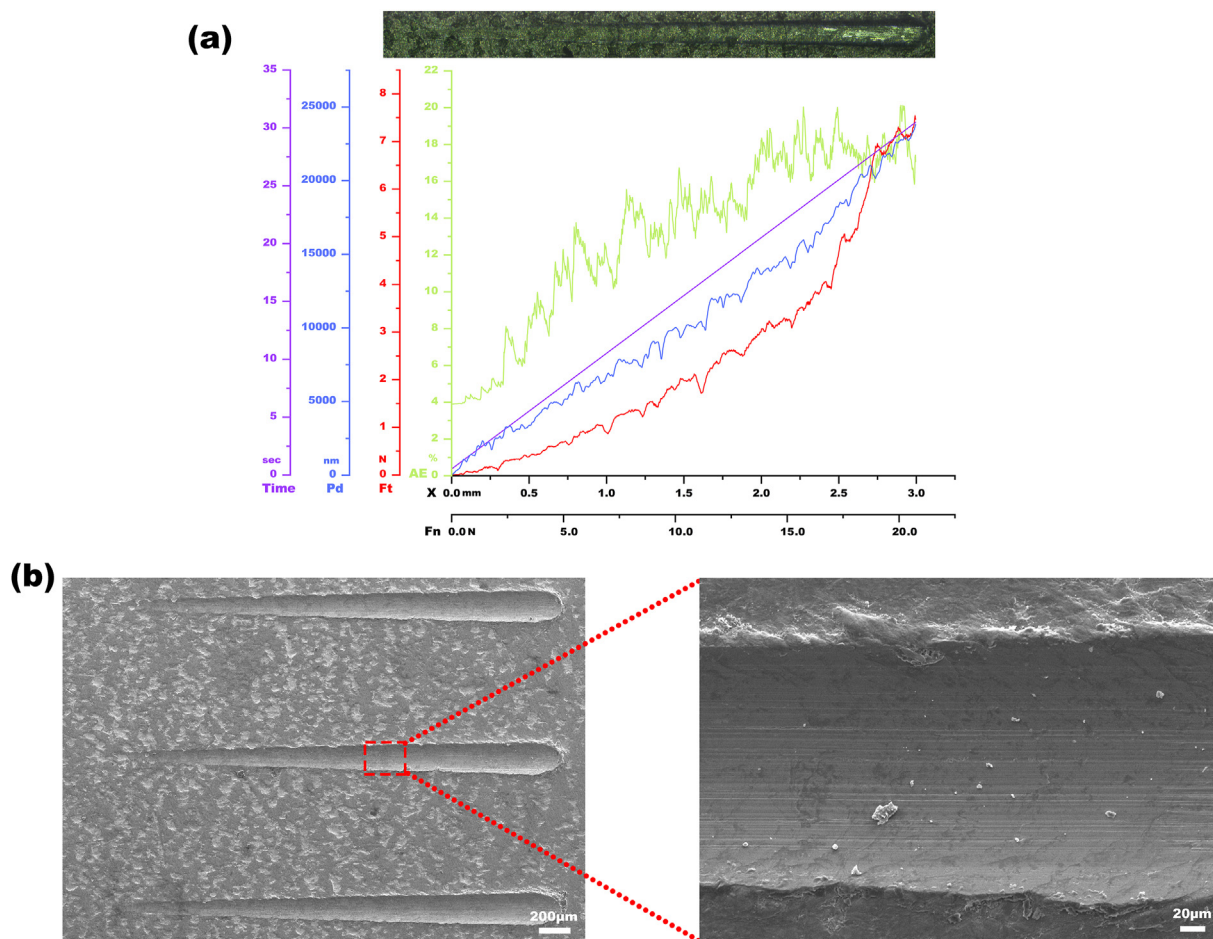


Fig. 4. The scratch testing combined with SEM for evaluation of coating on Ti-CCH. (a) The change of probing depth (Pd), scratching time, force of friction (Ft) and acoustical emission (AE) during the scratching process. (b) Low- and high-magnification SEM micrographs taken at the site of scratching on the surface of Ti-CCH substrates. Pd: probing depth, Ft: force of friction, AE: acoustical emission.

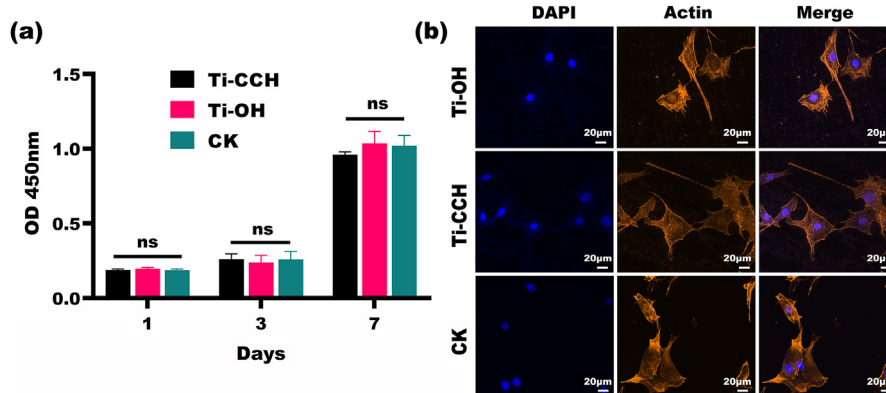


Fig. 5. Biocompatibility of Ti-CCH *in vitro*. (a) Cell proliferation of MC3T3-E1 preosteoblasts in Ti-CCH, Ti-OH and CK groups ($n = 3$). (b) Morphology of MC3T3-E1 preosteoblasts cultured for 1 day in Ti-CCH, Ti-OH and CK groups (red for F-actin and blue for cell nucleus). ns indicates no significant difference.

of different parameters during the scratching process. No abrupt change was observed along the scratching period. Fig. 4b shows low- and high-magnification SEM micrographs, respectively, taken on the top surface of the Ti-CCH coating at the location where scratch testing was conducted (progressively from left to right). The scratching was exerted by the conical diamond stylus with a load from 0.02 up to 20 N for a length about 3 mm, which introduced plastic deformation on the surface of Ti-CCH coating. However, neither microcracks nor areas of spalling in the coating could be observed around the scratch, which demonstrated the high strength of attachment of the coating to the titanium substrate, thereby meeting the requirements of the ASTM C1624-05 Standard (requiring resistance up to 20 N) for biomaterials' applications [45]. Hence, the first null hypothesis that "The QCMC/COL/HAP multilayer structure can not be constructed via modified LBL technique and poly dopamine binding methods" has to be rejected.

3.3. Biocompatibility assessment of Ti-CCH

In the aforementioned characterization method, different titanium samples were included in order to characterize the variation of surface properties during the characterization steps. While in the following cell or animal experiments, Ti-OH was selected as control group to reduce the random error due to the similar nano-grid surface compared to Ti-CCH according to previous studies [33,46]. The LBL multifilm coating was successfully fabricated and devoted to function on implant. Accordingly, the cytotoxicity of Ti-CCH should be thoroughly assessed to guarantee a good biocompatibility. In this study, MC3T3-E1 osteoblastic cells were employed to evaluate the biocompatibility of Ti-CCH *in vitro*. No significant difference was found among groups regarding the cells proliferation rate by using CCK-8 assay after cocultured for 1, 3 and 7 days (Fig. 5a). Moreover, fluorescent actin staining indicated that osteoblastic cells adequately stretched on both Ti substrates. As for Ti-CCH, cells exhibited an obvious elongated cytoskeleton (Fig. 5b). This can be attributed to the positively charged QCMC chain, with a high density of amino groups that promoted cell attachment and provided superior biocompatibility for the structure [37]. Therefore, Ti-CCH exhibited excellent biocompatibility and did not impair osteoblastic cells behavior.

To further evaluate the biocompatibility of Ti-CCH, an implant femoral model was constructed and the local as well as systemic reactions of SD rats were assessed. After implantation, the body weight of rats from Ti-OH and Ti-CCH groups continuously increased within 6 weeks and showed no significant difference (Fig. 6a). Blood examination indicated that the average level of NE was similar between the two groups at 3 and 6 weeks after surgery. The average level of HGB of Ti-CCH was lower than that of Ti-OH. However, no significant difference was found between Ti-OH and Ti-CCH groups regarding neutrophil and HGB levels (Fig. 6b). These results indicated that the systemic inflammatory

response induced by the implants were similar between groups. It had been demonstrated that hemolysis was one of the main challenges for the application of cationic surface coatings [47]. Nevertheless, our results showed that there was no significant difference regarding the level of HGB between Ti-OH and Ti-CCH groups, which might due to the blocking effect of the crosslinked COL I. Moreover, Fig. 6c shows the 3D images of femurs in Ti-OH and Ti-CCH groups by using Micro-CT reconstruction. The results indicated more new bone was generated in Ti-CCH group compared to that of Ti-OH. The quantitative analysis of generated new bone in the region of interest can be observed in Fig. 6d. As two main peri-implant bone tissue indexes, the values of BV/TV and Tb.Th in Ti-CCH group were significant higher than those of Ti-OH group. Bone histopathological analysis showed that an abundance of trabecular and hyperchromatic bone marrow cells were observed in peri-implant marrow cavities in both groups with more new bone deposition in Ti-CCH group (Fig. 6e). The results were consistent with cell evaluation *in vitro* and indicated that Ti-CCH can serve as a non-toxic and biocompatible implant.

3.4. Biodegradability of multifilm coating on Ti-CCH

It is known that the total stability of implants undergoes a trough at the first 4 weeks post-operation, for which a long-lasting antibacterial coating is required to guarantee a high success rate of implant. For traditional LBL technique, multilayer films formed by electrostatic interaction are usually unstable in physiological conditions [48]. In the present study, we employed a modified crosslinking LBL technique to form stable amido bonds [20]. Anthrone-sulfuric acid reaction had been demonstrated to be a useful method for carbohydrate detection with high sensitivity [49]. Therefore, our study utilized this method for the detection of the release of QCMC, and the result showed that our coating could serve as a reservoir for slow continuous release of QCMC for more than 45 days. Although Ti-CCH underwent a high-dose release of QCMC at first, it followed by a long-lasting release around 100–200 μg every two days. Moreover, nearly 88% of QCMC was released at the first month, reaching an amount of approximately 4377 ± 193 μg, while the remaining QCMC was continuously released at a low-dosage (Fig. 6f). It was revealed that wound and implant sites are rich in collagenase during the healing process, so that QCMC could be sustainably released under the action of collagenase *in vivo* [50]. Indeed, the collagenase simply used *in vitro* experiment was at a high concentration and was different from that of *in vivo* environment, where a series of factors including other proteases, local trauma, inflammation situation could influence the activity of collagenase. The interaction of the aforementioned factors finally decided the degradation of the multifilm coating. Thanks to this, the multifilms coating and QCMC were expected to be degraded for a longer period of time *in vivo* and exhibited a long-lasting antibacterial

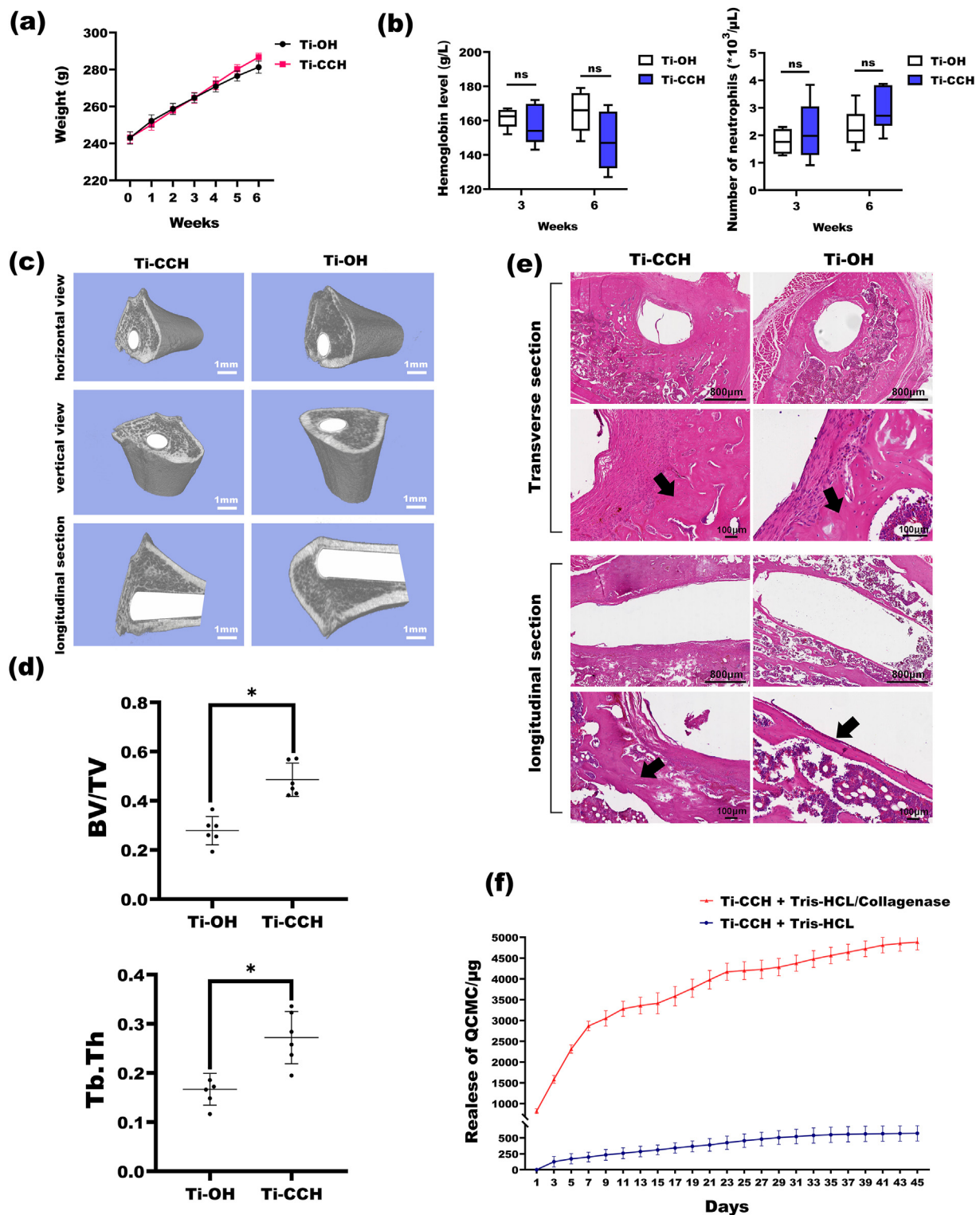


Fig. 6. Biocompatibility of Ti-CCH implant *in vivo* and the degradation of the coating under the action of collagenase. (a) The changes of body weight over time ($n = 5$). (b) Blood neutrophil and hemoglobin levels at 3 and 6 weeks ($n = 5$). (c) 3D reconstruction images of femurs with implants using Micro-CT. (d) Quantitative analysis from Micro-CT: the bone volume/total volume, BV/TV; the mean trabecular thickness, Tb.Th ($n = 5$). (e) Histological images of transverse and longitudinal sections from a femur stained with hematoxylin and eosin at 6 weeks. The black arrows indicate new bone formation around the implant. (f) Degradation of the coating under the action of collagenase *in vitro* ($n = 3$). * $P < 0.05$. ns indicated no significant difference.

effect. In this study, we conducted the *in vitro* collagenase experiments and the concentration of collagenase was 1 mg/mL as described in previous studies [19,51,52]. Therefore, the second null hypothesis that

“QCMC can not be slowly degraded from the multilayer structure for a long period of time” has to be rejected.

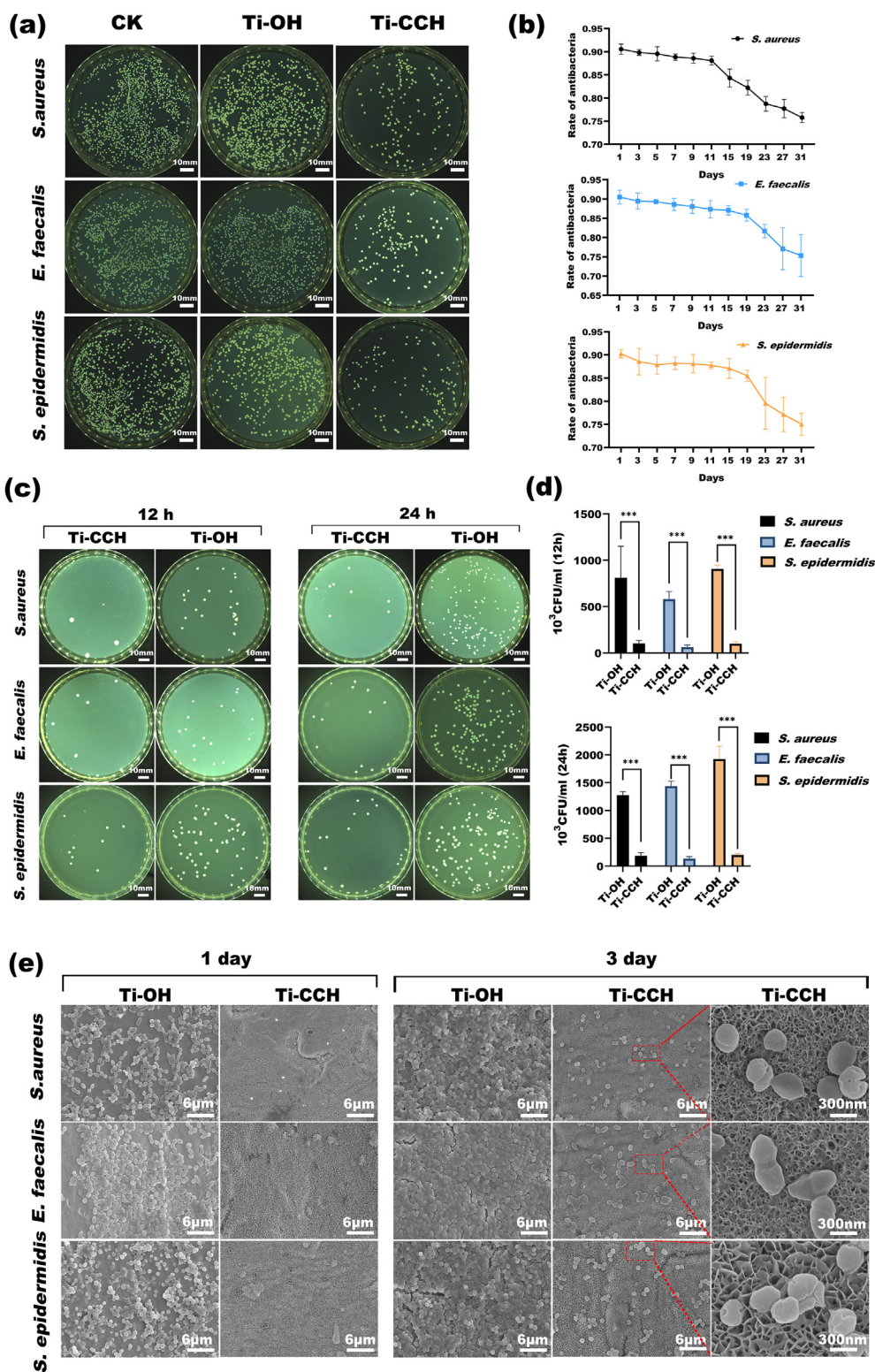


Fig. 7. Antibacterial effect of Ti-CCH *in vitro*. (a) Release-killing effect evaluated using spread plate method. (b) Quantitative analysis of the release-killing ratios against three bacteria (n = 3). (c) Contact-killing effect evaluated using spread plate method. (d) The number of viable bacteria adhered on the Ti-OH surface after cocultured for 12 h and 24 h (n = 3). (e) The adhesion and morphology of bacteria on the surfaces of different groups. ***P < 0.001.

3.5. Antibacterial activity *in vitro*

The colonization of bacteria on implant plays pivotal roles in the formation of bacterial biofilm. Once the biofilm has formed, bacteria would be protected against the host defence system and therapeutic agents. Moreover, the gene mutations of microorganism can be induced

and cause drug-resistance, leading to peri-implantitis [53]. Thus, there is a compelling need to pursue implants with an effective broad-spectrum antibacterial coating to eradicate infection rapidly in an early phase of post-operation. The antibacterial property of QCMC was endowed by the quaternary ammonium groups, which was positively charged and could bind to anionic bacterial membranes via electrostatic force, leading to

Table 4
Antibacterial rates of Ti-CCH evaluated in the contact-killing experiment.

| | <i>S. aureus</i> | <i>S. epidermidis</i> | <i>E. faecalis</i> |
|------|------------------|-----------------------|--------------------|
| 12 h | 86.5% | 88.8% | 88.7% |
| 24 h | 85.2% | 89.4% | 90.6% |

membrane disruption and cytoplasmic leakage [54]. The binding was nonspecific so that most of bacteria could be killed, and meanwhile drug-resistant infections could be prevented [55]. In our previous study, the antibacterial concentrations of QCMC against *Streptococcus mutans* (*S. mutans*) and *Enterococcus faecalis* (*E. faecalis*) were investigated, which indicated the desirable antibacterial ability of QCMC [35]. Data reported in the literature suggested that 67% of infections of implant were caused by *S. aureus* and *S. epidermidis*. The presence of the Staphylococcus bacteria in body could cause implant infections and biofilm formation at later times [42]. Furthermore, *S. aureus*, *S. epidermidis* and *E. faecalis* were commonly used as target bacteria for evaluating new antibacterial implant materials [56,57]. Among the 3 types of bacteria, *S. aureus* exhibited specific affinity for titanium surface with a strong virulence, which was the most common bacteria causing implant-related infections [58]. Therefore, *S. aureus* was used as a model bacteria for our long-lasting studies. As has been shown in the spread plate results, the rates of anti-*S. aureus*, *S. epidermidis* and *E. faecalis* in a medium were from 75.0% to 90.5% in the first month (Fig. 7a and b). This indicated that QCMC of Ti-CCH can be sustainably released to the surrounding environment and eradicated most bacteria with high risk for causing peri-implantitis. Even though a few bacteria broke through the anti-bacterial barrier and attached on the implant surface, 85.2% to 89.4% of *S. aureus* and *S. epidermidis* as well as 90.6% of *E. faecalis* would be killed by the remaining QCMC on the bottom layers of multifilm structures after cocultured for 24 h (Fig. 7c and d). The antibacterial rates against three bacteria in the contact-killing experiment were listed in Table 4. Based on the results of this investigation, it seems that our coatings constructed via the use of the covalently bonded LBL technique could be a promising antibacterial material with effective release-killing and contact-killing properties.

In addition, SEM was performed to visualize the anti-adhesion activity of Ti-CCH (Fig. 7e). After cocultured for 1 day, there were significantly more bacteria attached on Ti-OH compared to Ti-CCH. After 3 days, bacteria started interacting and aggregating to form biofilms on Ti-OH, while only a few bacteria attached to Ti-CCH with crumpled and ruptured membranes. Furthermore, Ti-CCH exhibited efficient bactericidal effect confirmed by live/dead staining (Fig. 8a). Green represented live bacteria, while red represented dead as well as membrane-damaged bacterial cells. The vast majority of three strains of bacteria were colored green on Ti-OH but red on Ti-CCH, revealing that Ti-CCH was developed with strong antibacterial capabilities. It's noteworthy that the total stability of implants undergoes a trough and the osteogenic interface is the weakest in the first 4 weeks post-operation, which becomes completely stable until 3 months [33]. Therefore, our expectation was that the antibacterial effect of implant coatings could last for at least 4 weeks and ideally more than 3 months. In order to evaluate the long-lasting antibacterial effect of Ti-CCH under physiological condition without high concentration of collagenase, *S. aureus* was chosen for investigation using the spread plate method. The results showed that the anti-*S. aureus* rate decreased from 92.7% to 88.8% in the first 3 weeks and remained 68.4% until 12 weeks (Fig. 8b). These results indicated that Ti-CCH provided a promising antibacterial effect along the healing process of implant.

3.6. In vivo evaluation of antibacterial activity of Ti-CCH

To further evaluate the antibacterial activity of Ti-CCH, an *in vivo* SD rat femoral infection model was constructed. After implanted for 4 weeks, the spread plate method was employed for detection of colonization bacteria of implants and the surrounding bone tissue (Fig. 9a). The

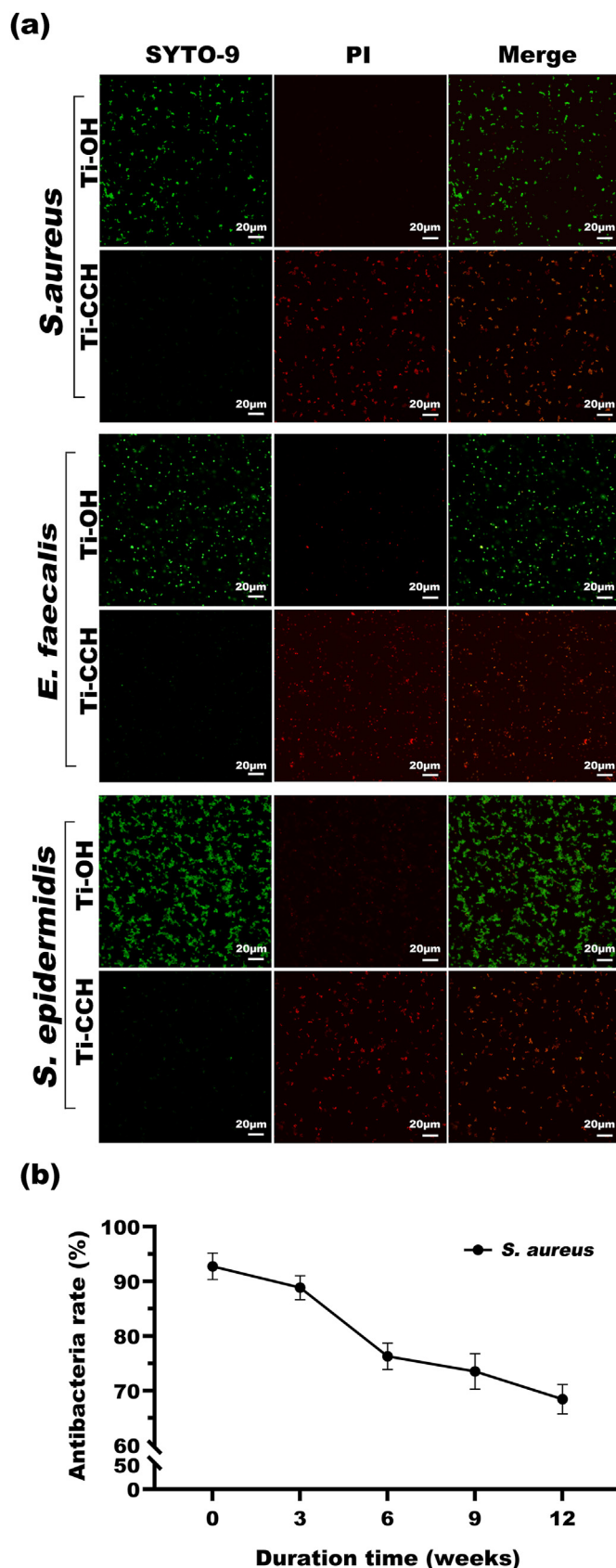


Fig. 8. Antibacterial effect of Ti-CCH *in vitro*. (a) Live/dead fluorescent detection of bacteria contacted with the coating (green fluorescence for live bacteria, red fluorescence for dead bacteria). (b) Long-lasting antibacterial ability of Ti-CCH against *S. aureus* (n = 3).

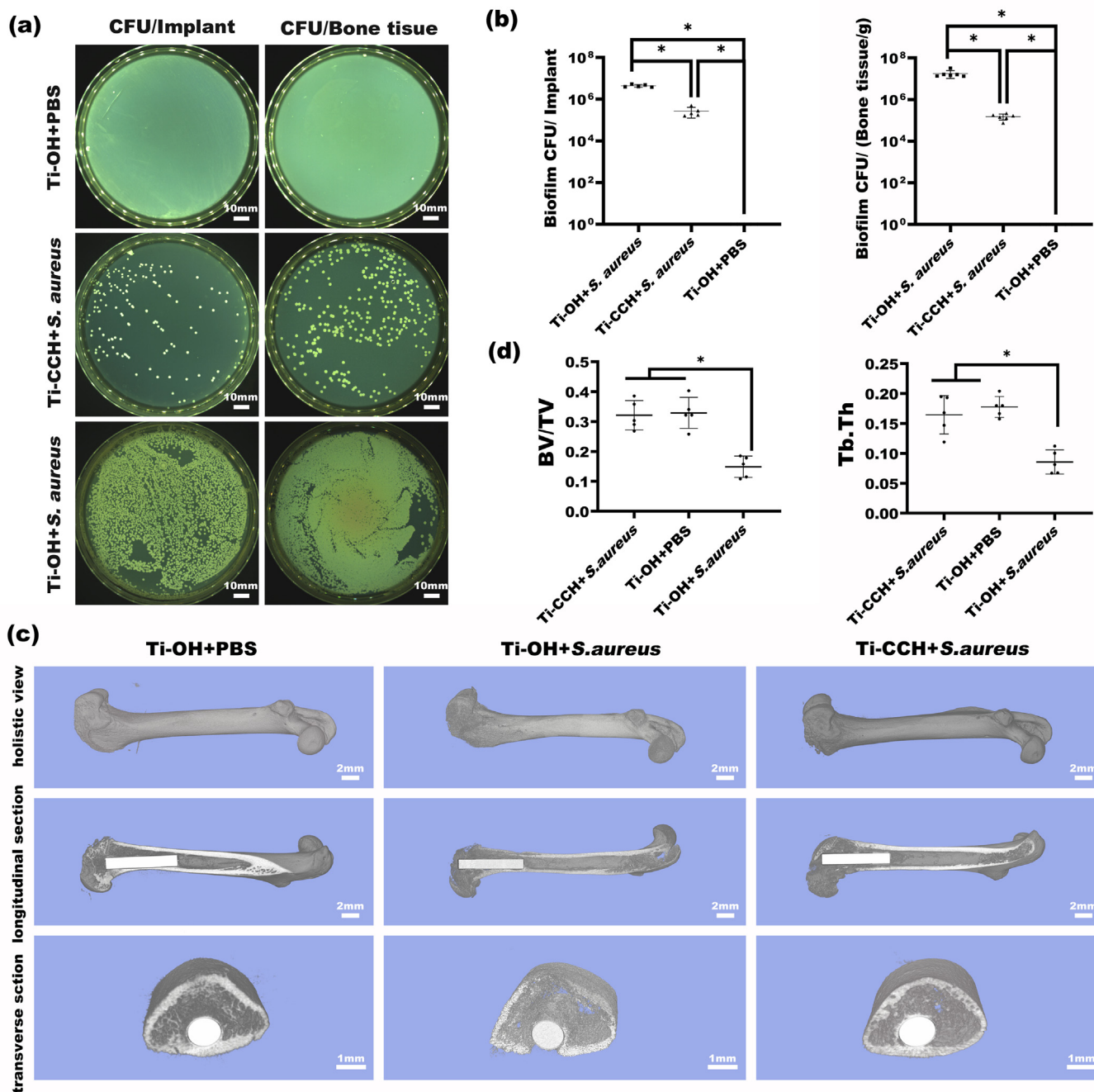


Fig. 9. Antibacterial effect of Ti-CCH implant *in vivo*. (a) In the rat femur infection model, the spread plate method was used to characterize the bacteria dwelling in the Ti rod and around the bone tissue after 4 weeks of post-operation. (b) The number of *S. aureus* adhered on the implant rods and the around bone tissue 4 weeks post-operation (n = 5). (c) 3D reconstruction images of femurs with implants using Micro-CT. (d) Quantitative analysis from Micro-CT: the bone volume/total volume, BV/TV; the mean trabecular thickness, Tb.Th (n = 5). *P < 0.05.

result showed that the number of colonies derived from bacteria adhered to implants and surrounding bone tissue in Ti-CCH+S.*aureus* group was significantly lower than that of Ti-OH+S.*aureus* group. No *S.aureus* colony was observed in Ti-OH+PBS group. The quantitative analysis was shown in Fig. 9b.

The infection of femur implant was detected by using Micro-CT and bone histopathological analysis. High resolution 3D images of femurs are shown in Fig. 9c. After implantation for 4 weeks, obvious osteolytic destruction was seen at the femoral condyles and cortical bone adjacent to implant site in the Ti-OH+S.*aureus* group. However, only slight osteolysis was observed in the Ti-CCH+S.*aureus* group and no obvious

abnormalities were shown in the Ti-OH+PBS group. Quantitative analysis of BV/TV and Tb.Th showed that no significant difference was found between the Ti-CCH+S.*aureus* group and the Ti-OH+PBS group, while the values of the Ti-OH+S.*aureus* group were the lowest (P < 0.05) (Fig. 9d). Bone histopathological analysis showed extensive cortical bone destruction with a large number of inflammatory cells in Ti-OH+S.*aureus* group after implantation for 4 weeks. Nevertheless, in the Ti-CCH+S.*aureus* group, fibrous tissue at peri-implant site was observed without a large number of inflammatory cells. Sequestrum was occasionally seen at longitudinal sections of the femurs. New bone tissue was also formed at peri-implant site in Ti-OH+PBS group without obvious

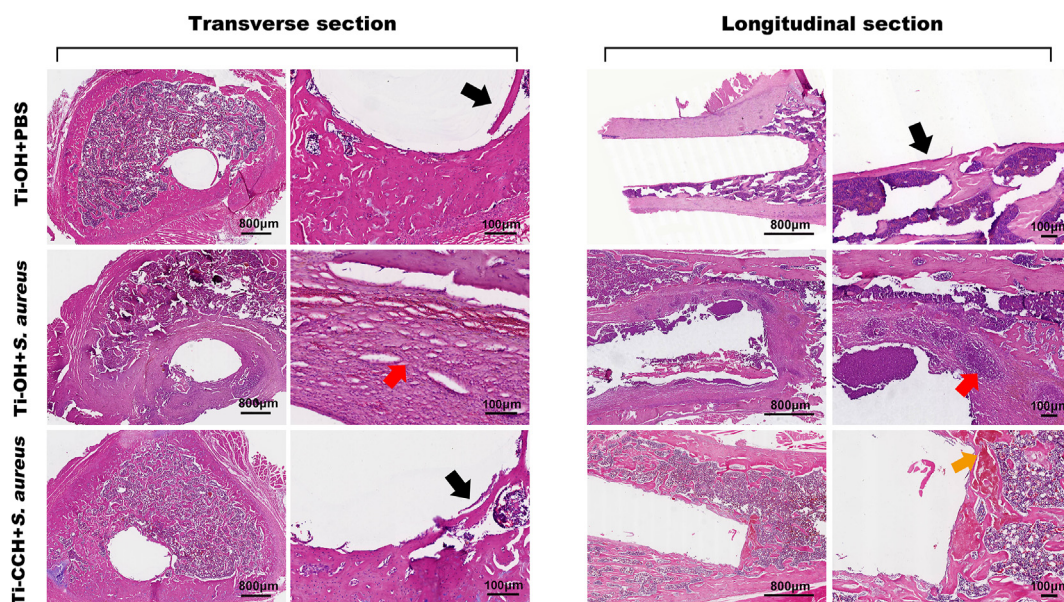


Fig. 10. Histological images of transverse and longitudinal sections from a femur stained with hematoxylin and eosin 4 weeks after implantation. The black arrows indicate new bone formation around the Ti implant. The red arrows indicate inflammatory tissue. The yellow arrow indicates sequestrum.

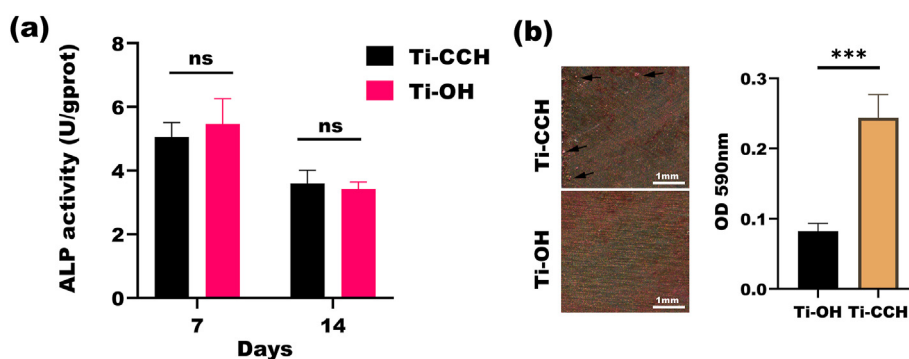


Fig. 11. Osteogenesis differentiation of MC3T3-E1 preosteoblasts on Ti-CCH substrates. (a) Alkaline phosphatase (ALP) detection after 7 and 14 days of osteogenic induction ($n = 3$). (b) Alizarin Red S staining and quantitative calculation after 28 days of osteogenic induction ($n = 3$) (Black arrows indicate mineralized nodules) *** $P < 0.001$, ns indicates no significant difference.

inflammatory response (Fig. 10). It has been demonstrated that the implantation of biomaterials could induce a tissue response around the implant site, which called locus minoris resistendiae and was susceptible to bacteria adhesion and infection [59,60]. As has been shown in the literature, the first 4 weeks after implantation was the peak phase of infection [61]. Based on the results of this investigation, Ti-CCH could effectively prevent infection during this high-risk period. Thus, the third null hypothesis that “The QCMC/COL/HAP multilayer structure has no long-lasting, multi-antibacterial effects and two-phase function” has to be partially rejected.

3.7. Osteogenesis activity of Ti-CCH *in vitro* and *in vivo*

After the first phase of high-risk infection, the osseointegration occurs and the second stability of implant starts building. Accordingly, biomaterials with desirable osteogenesis activity are paramount to set up the total stability of implant in advance and promote the healing of bone tissue [62]. In this study, HAP was crosslinked in our QCMC/COL/HAP coating to serve as an osteogenesis core [63,64]. According to the literature, MC3T3-E1 cells as precursors of osteoblasts are commonly used as the cell model in studying osteogenic development [65]. After cocultured with Ti-OH and Ti-CCH respectively for 7 and 14 days, there were no

significant differences regarding the alkaline phosphatase (ALP) activity between the two groups (Fig. 11a). However, scattered mineralized nodules were observed in Ti-CCH, whereas few red mineralized nodules can be seen in Ti-OH group after cocultured for 28 days. There was significant difference regarding the quantitative assay of alizarin red staining between groups (Fig. 11b). ALP was an enzyme produced by osteoblast and involved in the early bone mineralization process, while mineralization nodules are the later markers of osteoblastic differentiation [66]. In the early mineralization process, no significant activity of ALP was detected, which might be attributed to relatively insufficient number of HAP and blocking effect of the existing COL and QCMC biomacromolecules. HAP particles were covering in the nano-grid layer-by-layer structure. Therefore, with the degradation of multifilm coating, HAP particles were exposed and could interact with osteoblasts. After cocultured for 28 days, the upper films gradually degraded and the infection of implant could be prevented and controlled, thus enabling the second-phase function of HAP to induce osteogenesis.

To further evaluate the osteogenesis activity of Ti-CCH, an *in vivo* SD rat femoral infection model was constructed. After implanted for 8 weeks, the femurs of rats were collected and undergone Micro-CT scanning. High-resolution 3D images of the femurs are demonstrated in Fig. 12a. In Ti-OH+S.*aureus* group, peri-implant osteoporosis with less

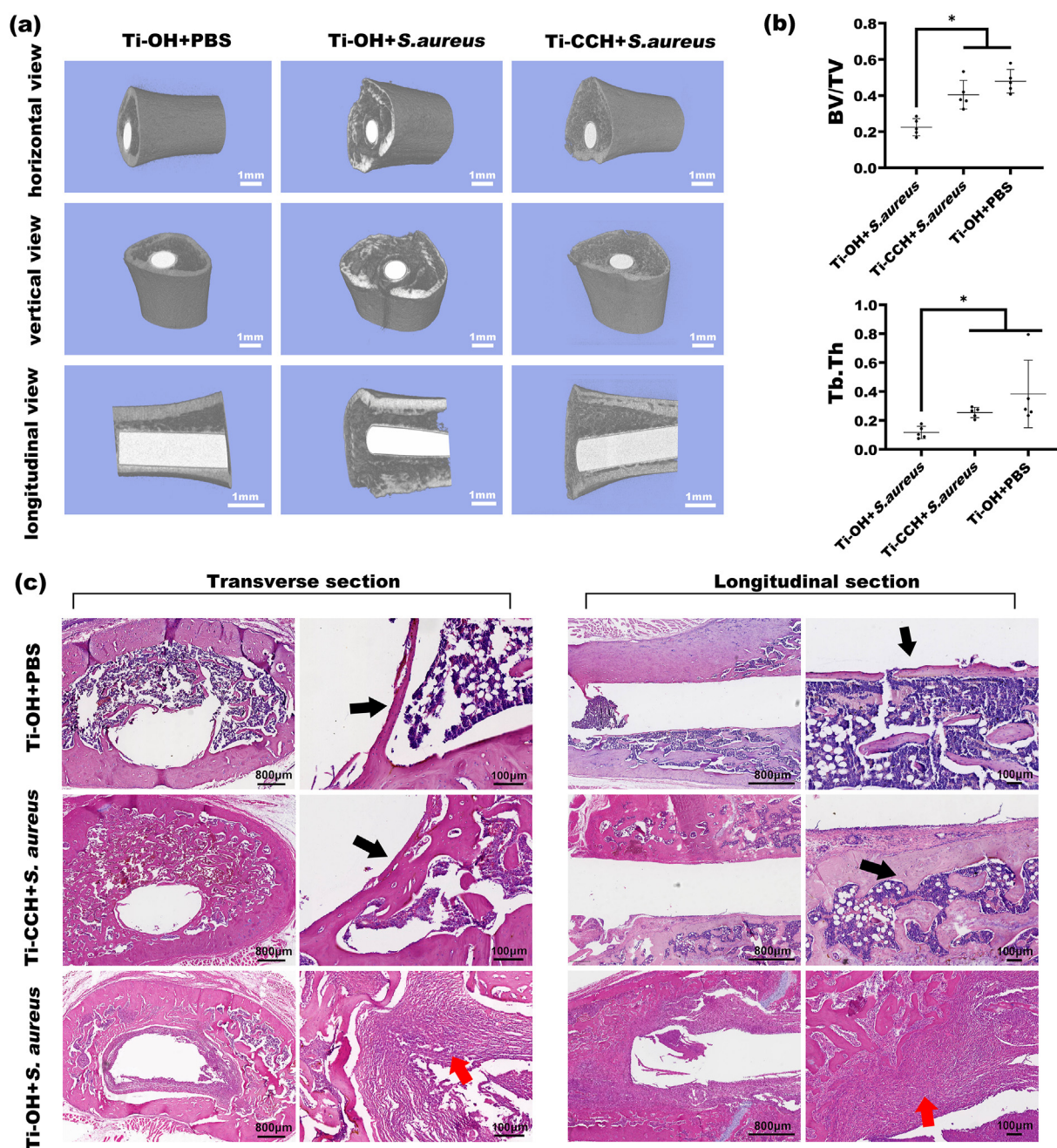


Fig. 12. Evaluation of osseointegration of Ti-CCH implants *in vivo*. (a) 3D reconstruction images of femurs with implants using Micro-CT. (b) Quantitative analysis from Micro-CT: the bone volume/total volume, BV/TV; the mean trabecular thickness, Tb.Th ($n = 5$). (c) Histological images of transverse and longitudinal sections from a femur stained with hematoxylin and eosin after implantation for 8 weeks. The black arrows indicate new bone formation around the Ti implant. The red arrows indicate inflammatory tissue. * $P < 0.05$.

trabecular number was observed. On the contrary, thicker bone substance and more trabecular number were seen in the Ti-CCH+S.aureus group. Quantitative analysis of BV/TV and Tb.Th indicated no significant difference between the Ti-CCH+S.aureus group and Ti-OH+PBS group, while both of them were higher than those of Ti-OH+S.aureus group ($P < 0.05$) (Fig. 12b). Bone histopathological analysis further showed extensive bone destruction with a large number of inflammatory cells infiltrated in tissue (red arrow) and no bone was formed in Ti-OH+S.aureus group. However, continuous cortical bone was observed and obvious new bone was formed (black arrow) in both Ti-CCH+S.aureus group and Ti-OH+PBS group (Fig. 12c). The Ti-CCH substrate constructed in this study owned a nano-grid structure, which is beneficial for cells adhesion and proliferation. Sequestrum could be observed in Ti-CCH+S.aureus group

(yellow arrow), which indicated that inflammation caused by the bacterial infection could lead to the necrosis of bone tissue, but was effectively controlled by QCMC on Ti-CCH. Then osteogenesis of implant was induced in the later stage, which were consistent with the two-staged function of our QCMC/COL/HAP coating. Therefore, our study proved that the QCMC/COL/HAP coating could enhance the generation of new bone around implant under the control of infection. According to the aforementioned results, the third null hypothesis was rejected. The present study mainly focused on the two-phased function of Ti-CCH implant. It proved that the modified LBL coating could exhibit multi-antibacterial effect during the phase of high-risk infection and then induce osteogenesis at the second phase, namely 4 weeks after implantation under the control of infection. Data reported in the literature suggested that bone

ingrowth into the porous coating at 3 months after surgery was sufficient to generate mechanical stability [67]. Based on the results of the SEM observation, the morphology of our coating was porous with a nano-grid structure. Thus, we surmised that the osseointegration could be favored through the improvement of mechanical interlock of bone growth into the porous implant structure [68,69]. Apart from the surface morphology, the mechanical stability of coating adhered on implant is important for the strength of osseointegration [70,71], which has been evaluated through the scratch test (Fig. 4). The results showed that the binding force of our coating was more than 20 N, which also provided the basis underlying the initial steps involved in achieving high-strength osseointegration. Nevertheless, the implant infection model employed in the present study was established in the femur of the SD rat rather than the alveolar bone of rabbit or dog, and mechanical pullout force test could not be conducted due to the limitation imposed by the current animal model [33]. Thus, much more work needs to be done to fully elucidate the strength of osseointegration in future studies by using big animal models.

4. Conclusions

In this work, we successfully fabricated a two-phase and long-lasting multi-antibacterial QCMC/COL/HAP coating utilizing the modified LBL technique and polymerization of dopamine. Based on the results of this investigation, it seems that the QCMC/COL/HAP coatings could be a promising antibacterial material with effective release-killing and contact-killing activities to eradicate infection rapidly during an early phase of post-operation. While the implant interface comes to the phase of osseointegration, it promoted bone formation and osteogenesis as well as maintaining a desirable antibacterial effect. The coating possessed desirable biocompatibility and could release QCMC for more than 45 days during the healing of implant, which was of great significance for developing practical implant and scaffold materials.

Credit author statement

Ruitian Lin contributed to data acquisition, analysis, interpretation and drafted the manuscript; Zhuoran Wang, contributed to data acquisition; Zihan Li, contributed to data acquisition; Lisha Gu, contributed to conception, design, interpretation and critically revised the manuscript. All authors gave final approval and agree to be accountable for all aspects of the work.

Data availability

All data are included in the manuscript and supplementary information appendix.

Declaration of competing interest

The authors declare that they have no known competing financial interests or personal relationships that could have appeared to influence the work reported in this paper.

Acknowledgement

This work was supported by the National Nature Science Foundation of China [grant number 81873712]; the Science and Technology Program of Guangzhou [grant number 201904010057]. We express our gratitude to Prof. Weichang Li from Guangdong Provincial Key Laboratory of Stomatology, Sun Yat-sen University for his guidance and support.

Appendix A. Supplementary data

Supplementary data to this article can be found online at <https://doi.org/10.1016/j.mtbio.2022.100330>.

References

- [1] L.N. Ikryannikova, M.V. Malakhova, G.G. Lominadze, I.Y. Karpova, E.S. Kostryukova, N.A. Mayansky, A.N. Kruglov, E.A. Klimova, E.S. Lisitsina, E.N. Iliina, V.M. Govorun, Inhibitory effect of streptococci on the growth of *M. catarrhalis* strains and the diversity of putative bacteriocin-like gene loci in the genomes of *S. pneumoniae* and its relatives, *AMB Express* 7 (2017), <https://doi.org/10.1186/s13568-017-0521-z>, 218–218.
- [2] S.A. Jalil, M. Akram, J.A. Bhat, J.J. Hayes, S.C. Singh, M. Elkabbash, C. Guo, Creating superhydrophobic and antibacterial surfaces on gold by femtosecond laser pulses, *Appl. Surf. Sci.* 506 (2020), <https://doi.org/10.1016/j.apsusc.2019.144952>, 144952–144952.
- [3] V.P.P. Alonso, A.M.M. Harada, D.Y. Kabuki, Competitive and/or cooperative interactions of *Listeria monocytogenes* with *Bacillus cereus* in dual-species biofilm formation, *Front. Microbiol.* 11 (2020), <https://doi.org/10.3389/fmicb.2020.00177>, 177–177.
- [4] A. Escobar, N. Muzzio, S.E. Moya, Antibacterial layer-by-layer coatings for medical implants, *Pharmaceutics* 13 (2020) 16, <https://doi.org/10.3390/pharmaceutics13010016>.
- [5] J. Yang, H. Zhang, S.M. Chan, R. Li, Y. Wu, M. Cai, A. Wang, Y. Wang, TiO₂ nanotubes alleviate diabetes-induced osteogenic inhibition, *Int. J. Nanomed.* 15 (2020) 3523–3537, <https://doi.org/10.2147/IJN.S237008>.
- [6] O. Camps-Font, R. Figueiredo, E. Valmaseda-Castellon, C. Gay-Escoda, Postoperative infections after dental implant placement: prevalence, clinical features, and treatment, *Implant Dent.* 24 (2015) 713–719, <https://doi.org/10.1097/ID.0000000000000325>.
- [7] J. Ballarre, T. Aydemir, L. Liverani, J.A. Roether, W.H. Goldmann, A.R. Boccaccini, Versatile bioactive and antibacterial coating system based on silica, gentamicin, and chitosan: improving early stage performance of titanium implants, *Surf. Coat. Technol.* 381 (2020), <https://doi.org/10.1016/j.surfcoat.2019.125138>.
- [8] M. Stevanovic, M. Djosic, A. Jankovic, K. Nesovic, V. Kojic, J. Stojanovic, S. Grujic, I.M. Bujagic, K.Y. Rhee, V. Miskovic-Stankovic, Assessing the bioactivity of gentamicin-preloaded hydroxyapatite/chitosan composite coating on titanium substrate, *ACS Omega* 5 (2020) 15433–15445, <https://doi.org/10.1021/acsomega.0c01583>.
- [9] M. Zhu, X. Liu, L. Tan, Z. Cui, Y. Liang, Z. Li, K.W. Kwok, Y. Wu, Photo-responsive chitosan/Ag/MoS₂ for rapid bacteria-killing, *J. Hazard. Mater.* 383 (2020), 121122, <https://doi.org/10.1016/j.jhazmat.2019.121122>.
- [10] S. Amin Yavari, L. Loozen, F.L. Paganelli, S. Bakhshandeh, K. Liettaert, J.A. Groot, A.C. Fluit, C.H. Boel, J. Alblas, H.C. Vogely, H. Weinans, A.A. Zadpoor, Antibacterial behavior of additively manufactured porous titanium with nanotubular surfaces releasing silver ions, *ACS Appl. Mater. Interfaces* 8 (2016) 17080–17089, <https://doi.org/10.1021/acami.6b03152>.
- [11] A. Pérez-Anes, M. Gargouri, W. Laure, H. Van Den Berghe, E. Courcot, J. Sobocinski, N. Tabary, F. Chai, J.F. Blach, A. Addad, P. Woisel, D. Douroumis, B. Martel, N. Blanchemain, J. Lyskawa, Bioinspired titanium drug eluting platforms based on a pol-β-cyclodextrin-chitosan layer-by-layer self-assembly targeting infections, *ACS Appl. Mater. Interfaces* 7 (2015) 12882–12893, <https://doi.org/10.1021/acami.5b02402>.
- [12] N.J. Hickok, I.M. Shapiro, Immobilized antibiotics to prevent orthopaedic implant infections, *Adv. Drug Deliv. Rev.* 64 (2012) 1165–1176, <https://doi.org/10.1016/j.addr.2012.03.015>.
- [13] W. Zhou, X. Peng, Y. Ma, Y. Hu, Y. Wu, F. Lan, M.D. Weir, M. Li, B. Ren, T.W. Oates, H.H.K. Xu, X. Zhou, L. Cheng, Two-staged time-dependent materials for the prevention of implant-related infections, *Acta Biomater.* 101 (2020) 128–140, <https://doi.org/10.1016/j.actbio.2019.10.023>.
- [14] W.H. Kim, J.-C. Lee, D. Lim, Y.-K. Heo, E.-S. Song, Y.-J. Lim, B. Kim, Optimized dental implant fixture design for the desirable stress distribution in the surrounding bone region: a biomechanical analysis, *Materials* 12 (2019) 2749, <https://doi.org/10.3390/ma12172749>.
- [15] B. Lohberger, N. Stuehl, D. Glaenger, B. Rinner, N. Donohue, H.C. Lichtenegger, L. Ploszczanski, A. Leithner, CoCrMo surface modifications affect biocompatibility, adhesion, and inflammation in human osteoblasts, *Sci. Rep.* 10 (2020) 1682, <https://doi.org/10.1038/s41598-020-58742-9>.
- [16] P. Schupbach, R. Glauser, S. Bauer, Al₂O₃ particles on titanium dental implant systems following sandblasting and acid-etching process, *Int. J. Biomater.* 2019 (2019), 6318429, <https://doi.org/10.1155/2019/6318429>.
- [17] G. Decher, J.D. Hong, J. Schmitt, Buildup of ultrathin multilayer films by a self-assembly process: III. Consecutively alternating adsorption of anionic and cationic polyelectrolytes on charged surfaces, *Thin Solid Films* 210–211 (1992) 831–835, [https://doi.org/10.1016/0040-6090\(92\)90417-A](https://doi.org/10.1016/0040-6090(92)90417-A).
- [18] S. Abalde-Cela, P. Aldeanueva-Potel, C. Mateo-Mateo, L. Rodriguez-Lorenzo, R.A. Alvarez-Puebla, L.M. Liz-Marzan, Surface-enhanced Raman scattering biomedical applications of plasmonic colloidal particles, *J. R. Soc. Interface* 7 (Suppl 4) (2010) S435–S450, <https://doi.org/10.1098/rsif.2010.0125.focus>.
- [19] H. Ao, S. Yang, B. Nie, Q. Fan, Q. Zhang, J. Zong, S. Guo, X. Zheng, T. Tang, Improved antibacterial properties of collagen I/hyaluronic acid/quaternized chitosan multilayer modified titanium coatings with both contact-killing and release-killing functions, *J. Mater. Chem. B* 7 (2019) 1951–1961, <https://doi.org/10.1039/c8tb02425a>.
- [20] H. Ao, Y. Xie, H. Tan, S. Yang, K. Li, X. Wu, X. Zheng, T. Tang, Fabrication and in vitro evaluation of stable collagen/hyaluronic acid biomimetic multilayer on titanium coatings, *J. R. Soc. Interface* 10 (2013), <https://doi.org/10.1098/rsif.2013.0070>, 20130070–20130070.
- [21] L. Suo, N. Jiang, Y. Wang, P. Wang, J. Chen, X. Pei, J. Wang, Q. Wan, The enhancement of osseointegration using a graphene oxide/chitosan/hydroxyapatite

- composite coating on titanium fabricated by electrophoretic deposition, *J. Biomed. Mater. Res. B Appl. Biomater.* 107 (2019) 635–645, <https://doi.org/10.1002/jbm.b.34156>.
- [22] X.Y. Li, B.O. Liu, X.Y. Wang, Y. Han, H.J. Su, X.J. Zeng, R.C. Sun, Synthesis, characterization and antioxidant activity of quaternized carboxymethyl chitosan oligosaccharides, *J. Macromol. Sci. A* 49 (2012) 861–868, <https://doi.org/10.1080/10601325.2012.714679>.
- [23] G.M. Cunniffe, C.M. Curtin, E.M. Thompson, G.R. Dickson, F.J. O'Brien, Content-dependent osteogenic response of nanohydroxyapatite: an in vitro and in vivo assessment within collagen-based scaffolds, *ACS Appl. Mater. Interfaces* 8 (2016) 23477–23488, <https://doi.org/10.1021/acsmi.6b06596>.
- [24] P.P. Patel, C. Buckley, B.L. Taylor, C.C. Sahyoun, S.D. Patel, A.J. Mont, L. Mai, S. Patel, J.W. Freeman, Mechanical and biological evaluation of a hydroxyapatite-reinforced scaffold for bone regeneration, *J. Biomed. Mater. Res. A* 107 (2019) 732–741, <https://doi.org/10.1002/jbm.a.36588>.
- [25] W. Wang, K.W.K. Yeung, Bone grafts and biomaterials substitutes for bone defect repair: a review, *Bioact. Mater.* 2 (2017) 224–247, <https://doi.org/10.1016/j.bioactmat.2017.05.007>.
- [26] Y. Li, W. Yang, X. Li, X. Zhang, C. Wang, X. Meng, Y. Pei, X. Fan, P. Lan, C. Wang, X. Li, Z. Guo, Improving osteointegration and osteogenesis of three-dimensional porous Ti6Al4V scaffolds by polydopamine-assisted biomimetic hydroxyapatite coating, *ACS Appl. Mater. Interfaces* 7 (2015) 5715–5724, <https://doi.org/10.1021/acsmi.5b00331>.
- [27] C.Y. Chien, W.B. Tsai, Poly(dopamine)-assisted immobilization of Arg-Gly-Asp peptides, hydroxyapatite, and bone morphogenic protein-2 on titanium to improve the osteogenesis of bone marrow stem cells, *ACS Appl. Mater. Interfaces* 5 (2013) 6975–6983, <https://doi.org/10.1021/am401071f>.
- [28] X. Zhu, X. Zhou, J. Yi, J. Tong, H. Wu, L. Fan, Preparation and biological activity of quaternized carboxymethyl chitosan conjugated with collagen peptide, *Int. J. Biol. Macromol.* 70 (2014) 300–305, <https://doi.org/10.1016/j.ijbiomac.2014.06.045>.
- [29] N. Rajan, J. Habermehl, M.F. Coté, C.J. Doillon, D. Mantovani, Preparation of ready-to-use, storable and reconstituted type I collagen from rat tail tendon for tissue engineering applications, *Nat. Protoc.* 1 (2006) 2753–2758, <https://doi.org/10.1038/nprot.2006.430>.
- [30] B. Nie, H. Ao, T. Long, J. Zhou, T. Tang, B. Yue, Immobilizing bacitracin on titanium for prophylaxis of infections and for improving osteoinductivity: an in vivo study, *Colloids Surf. B Biointerfaces* 150 (2017) 183–191, <https://doi.org/10.1016/j.colsurfb.2016.11.034>.
- [31] M. Diefenbeck, C. Schrader, F. Gras, T. Muckley, J. Schmidt, S. Zankovych, J. Bossert, K.D. Jandt, A. Volpel, B.W. Sigusch, H. Schubert, S. Bischoff, W. Pfister, B. Edel, M. Faucon, U. Finger, Gentamicin coating of plasma chemical oxidized titanium alloy prevents implant-related osteomyelitis in rats, *Biomaterials* 101 (2016) 156–164, <https://doi.org/10.1016/j.biomaterials.2016.05.039>.
- [32] R.E. Weber, J.J. Petkowski, B. Michaels, K. Wisniewski, A. Piela, S. Antoszczak, M.U. Weber, Fluid-Screen as a real time dielectrophoretic method for universal microbial capture, *Sci. Rep.* 11 (2021), 22222, <https://doi.org/10.1038/s41598-021-01600-z>.
- [33] S. Wu, J. Xu, L. Zou, S. Luo, R. Yao, B. Zheng, G. Liang, D. Wu, Y. Li, Long-lasting renewable antibacterial porous polymeric coatings enable titanium biomaterials to prevent and treat peri-implant infection, *Nat. Commun.* 12 (2021) 3303, <https://doi.org/10.1038/s41467-021-23069-0>.
- [34] B. Liu, X.Y. Wang, B. Yang, R.C. Sun, Microwave-assisted synthesis of quaternized carboxymethyl chitosan in aqueous solution and its thermal behavior, *J. Macromol. Sci. A* 49 (2012) 227–234, <https://doi.org/10.1080/10601325.2012.649191>.
- [35] T. Shan, L. Huang, F.R. Tay, L. Gu, Retention of intrafibrillar minerals improves resin-dentin bond durability, *J. Dent. Res.* (2022), <https://doi.org/10.1177/00220345221103137>.
- [36] H. Ao, T. Tang, X. Zheng, Preparation and properties of hacc-based multilayers modified titanium coatings, *J. Orthop. Translat.* 7 (2016) 77, <https://doi.org/10.1016/j.jot.2016.06.034>.
- [37] A. Hashemi, M. Ezati, J. Mohammadnejad, B. Houshmand, S. Faghihi, Chitosan coating of TiO₂ nanotube arrays for improved metformin release and osteoblast differentiation, *Int. J. Nanomed.* 15 (2020) 4471–4481, <https://doi.org/10.2147/ijn.S248927>.
- [38] K. Zhang, Y. Zhuang, W. Zhang, Y. Guo, X. Liu, Functionalized MoS₂-nanoparticles for transdermal drug delivery of atenolol, *Drug Deliv.* 27 (2020) 909–916, <https://doi.org/10.1080/10717544.2020.1778815>.
- [39] X. Zhang, J. Chen, X. Pei, J. Wang, Q. Wan, S. Jiang, C. Huang, X. Pei, Enhanced osseointegration of porous titanium modified with zeolitic imidazole framework-8, *ACS Appl. Mater. Interfaces* 9 (2017) 25171–25183, <https://doi.org/10.1021/acsmi.7b07800>.
- [40] X. Shen, Y. Zhang, P. Ma, L. Sutrisno, Z. Luo, Y. Hu, Y. Yu, B. Tao, C. Li, K. Cai, Fabrication of magnesium/zinc-metal organic framework on titanium implants to inhibit bacterial infection and promote bone regeneration, *Biomaterials* 212 (2019) 1–16, <https://doi.org/10.1016/j.biomaterials.2019.05.008>.
- [41] D. Inoue, T. Kabata, K. Ohtani, Y. Kajino, T. Shirai, H. Tsuchiya, Inhibition of biofilm formation on iodine-supported titanium implants, *Int. Orthop.* 41 (2017) 1093–1099, <https://doi.org/10.1007/s00264-017-3477-3>.
- [42] V. Zarghami, M. Ghorbani, K.P. Bagheri, M.A. Shokrgozar, Prolongation of bactericidal efficiency of chitosan - bioactive glass coating by drug controlled release, *Prog. Org. Coating* 139 (2020), 10544, <https://doi.org/10.1016/j.porgcoat.2019.105440>.
- [43] M. Seyhan, O. Guler, M. Mahirogullari, F. Donmez, A. Gereli, S. Mutlu, Complications during removal of stainless steel versus titanium nails used for intramedullary nailing of diaphyseal fractures of the tibia, *Ann. Surg.* 26 (2018) 38–42, <https://doi.org/10.1016/j.amsu.2017.12.012>.
- [44] A.T. Celebi, E. Icer, M.M. Eren, C. Baykasoglu, A. Mugan, E. Yildiz, Thermal-stress analysis of ceramic laminate veneer restorations with different incisal preparations using micro-computed tomography-based 3D finite element models, *J. Mech. Behav. Biomed. Mater.* 75 (2017) 302–313, <https://doi.org/10.1016/j.jmbmb.2017.07.039>.
- [45] P.A. West Conshohocken, C1624-2005 Standard Test Method for Adhesion Strength and Mechanical Failure Modes of Ceramic Coatings by Quantitative Single Point Scratch Testing, vol. 15, ASTM International, 2015, <https://doi.org/10.1520/C1624-05R15>, 03.
- [46] W. Li, Y.W. Yang, H.C. Zhang, Z.X. Xu, L.B. Zhao, J.Q. Wang, Y.N. Qiu, B. Liu, Improvements on biological and antimicrobial properties of titanium modified by AgNPs-loaded chitosan-heparin polyelectrolyte multilayers, *J. Mater. Sci. Mater. Med.* 30 (2019) <https://doi.org/10.1007/s10856-019-6250-x>.
- [47] X.L. Fan, M. Hu, Z.H. Qin, J. Wang, X.C. Chen, W.X. Lei, W.Y. Ye, Q. Jin, K.F. Ren, J. Ji, Bactericidal and hemocompatible coating via the mixed-charged copolymer, *ACS Appl. Mater. Interfaces* 10 (2018) 10428–10436, <https://doi.org/10.1021/acsmi.7b18889>.
- [48] Y. Huang, Q. Luo, X. Li, F. Zhang, S. Zhao, Fabrication and in vitro evaluation of the collagen/hyaluronic acid PEM coating crosslinked with functionalized RGD peptide on titanium, *Acta Biomater.* 8 (2012) 866–877, <https://doi.org/10.1016/j.actbio.2011.10.020>.
- [49] A. Leyva, A. Quintana, M. Sanchez, E.N. Rodriguez, J. Cremata, J.C. Sanchez, Rapid and sensitive anthrone-sulfuric acid assay in microplate format to quantify carbohydrate in biopharmaceutical products: method development and validation, *Biologicals* 36 (2008) 134–141, <https://doi.org/10.1016/j.jbiologicals.2007.09.001>.
- [50] S.M. McCarty, S.L. Percival, Proteases and delayed wound healing, *Adv. Wound Care* 2 (2013) 438–447, <https://doi.org/10.1089/wound.2012.0370>.
- [51] H. Ao, Y. Xie, H. Tan, X. Wu, G. Liu, A. Qin, X. Zheng, T. Tang, Improved hMSC functions on titanium coatings by type I collagen immobilization, *J. Biomed. Mater. Res. A* 102 (2014) 204–214, <https://doi.org/10.1002/jbm.a.34682>.
- [52] R. Muller, J. Abke, E. Schnell, D. Scharnweber, R. Kujat, C. Englert, D. Taheri, M. Nerlich, P. Angele, Influence of surface pretreatment of titanium- and cobalt-based biomaterials on covalent immobilization of fibrillar collagen, *Biomaterials* 27 (2006) 4059–4068, <https://doi.org/10.1016/j.biomaterials.2006.03.019>.
- [53] C.R. Ariola, D. Campoccia, L. Montanaro, Implant infections: adhesion, biofilm formation and immune evasion, *Nat. Rev. Microbiol.* 16 (2018) 397–409, <https://doi.org/10.1038/s41579-018-0019-y>.
- [54] J.M. Antonucci, D.N. Zeiger, K. Tang, S. Lin-Gibson, B.O. Fowler, N.J. Lin, Synthesis and characterization of dimethacrylates containing quaternary ammonium functionalities for dental applications, *Dent. Mater.* 28 (2012) 219–228, <https://doi.org/10.1016/j.dental.2011.10.004>.
- [55] S. Wang, H. Wang, B. Ren, X. Li, L. Wang, H. Zhou, M.D. Weir, X. Zhou, R.M. Masri, T.W. Oates, L. Cheng, H.H.K. Xu, Drug resistance of oral bacteria to new antibacterial dental monomer dimethylaminohexadecyl methacrylate, *Sci. Rep.* 8 (2018) 5509, <https://doi.org/10.1038/s41598-018-23831-3>.
- [56] A.L. Overmann, C. Aparicio, J.T. Richards, I. Mutreja, N.G. Fischer, S.M. Wade, B.K. Potter, T.A. Davis, J.E. Bechtold, J.A. Forsberg, D. Dey, Orthopaedic osseointegration: implantology and future directions, *J. Orthop. Res.* 38 (2020) 1445–1454, <https://doi.org/10.1002/jor.24576>.
- [57] F. Parnia, J. Yazdani, V. Javaherzadeh, S.M. Dizaj, Overview of nanoparticle coating of dental implants for enhanced osseointegration and antimicrobial purposes, *J. Pharm. Pharmaceut. Sci.* 20 (2017) 148–160, <https://doi.org/10.18433/J3gp6g>.
- [58] D.M. Brunette, P. Tengvall, M. Textor, P. Thomsen, Titanium in Medicine: Material Science, Surface Science, Engineering, Biological Responses and Medical Applications, Springer Science & Business Media, Berlin, 2012.
- [59] J.M. Schierholz, J. Beuth, Implant infections: a haven for opportunistic bacteria, *J. Hosp. Infect.* 49 (2001) 87–93, <https://doi.org/10.1053/jhin.2001.1052>.
- [60] D.A. Siddiqui, L. Guida, S. Sridhar, P. Valderrama, T.G. Wilson, D.C. Rodrigues, Evaluation of oral microbial corrosion on the surface degradation of dental implant materials, *J. Periodontol.* 90 (2019) 72–81, <https://doi.org/10.1002/Jper.18-0110>.
- [61] P.I. Branemark, Osseointegration and its experimental background, *J. Prosthet. Dent.* 50 (1983) 399–410, [https://doi.org/10.1016/s0022-3913\(83\)80101-2](https://doi.org/10.1016/s0022-3913(83)80101-2).
- [62] R. Marsell, T.A. Einhorn, The biology of fracture healing, *Injury* 42 (2011) 551–555, <https://doi.org/10.1016/j.injury.2011.03.031>.
- [63] J. Chen, P. Pan, Y. Zhang, S. Zhong, Q. Zhang, Preparation of chitosan/nano hydroxyapatite organic-inorganic hybrid microspheres for bone repair, *Colloids Surf. B Biointerfaces* 134 (2015) 401–407, <https://doi.org/10.1016/j.colsurfb.2015.06.072>.
- [64] X. Guo, J.E. Gough, P. Xiao, J. Liu, Z. Shen, Fabrication of nanostructured hydroxyapatite and analysis of human osteoblastic cellular response, *J. Biomed. Mater. Res. A* 82 (2007) 1022–1032, <https://doi.org/10.1002/jbm.a.31200>.
- [65] A.A. Fatokun, T.W. Stone, R.A. Smith, Responses of differentiated MC3T3-E1 osteoblast-like cells to reactive oxygen species, *Eur. J. Pharmacol.* 587 (2008) 35–41, <https://doi.org/10.1016/j.ejphar.2008.03.024>.
- [66] T. Yonezawa, J.W. Lee, A. Hibino, M. Asai, H. Hojo, B.Y. Cha, T. Teruya, K. Nagai, U.I. Chung, K. Yagasaki, J.T. Woo, Harmine promotes osteoblast differentiation through bone morphogenetic protein signaling, *Biochem. Biophys. Res. Commun.* 409 (2011) 260–265, <https://doi.org/10.1016/j.bbrc.2011.05.001>.
- [67] S. Jeyapalina, J.P. Beck, R.D. Bloebaum, K.N. Bachus, Progression of bone ingrowth and attachment strength for stability of percutaneous osseointegrated prostheses, *Clin. Orthop.* 472 (2014) 2957–2965, <https://doi.org/10.1007/s11999-013-3381-0>.
- [68] W. Peng, L. Xu, J. You, L. Fang, Q. Zhang, Selective laser melting of titanium alloy enables osseointegration of porous multi-rooted implants in a rabbit model, *Biomed. Eng. Online* 15 (2016) 85, <https://doi.org/10.1186/s12938-016-0207-9>.

- [69] J. Matena, S. Petersen, M. Gieseke, A. Kampmann, M. Teske, M. Beyerbach, H. Murua Escobar, H. Haferkamp, N.-C. Gellrich, I. Nolte, SLM produced porous titanium implant improvements for enhanced vascularization and osteoblast seeding, *Int. J. Mol. Sci.* 16 (2015) 7478–7492, <https://doi.org/10.3390/ijms16047478>.
- [70] X. Tang, K. Huang, J. Dai, Z. Wu, L. Cai, L. Yang, J. Wei, H. Sun, Influences of surface treatments with abrasive paper and sand-blasting on surface morphology, hydrophilicity, mineralization and osteoblasts behaviors of n-CS/PK composite, *Sci. Rep.* 7 (2017) 568, <https://doi.org/10.1038/s41598-017-00571-4>.
- [71] W.W. Lou, Y.W. Dong, H.L. Zhang, Y.F. Jin, X.H. Hu, J.F. Ma, J.S. Liu, G. Wu, Preparation and characterization of lanthanum-incorporated hydroxyapatite coatings on titanium substrates, *Int. J. Mol. Sci.* 16 (2015) 21070–21086, <https://doi.org/10.3390/ijms160921070>.